



## RESEARCH ARTICLE

10.1029/2023JD038873

### Special Section:

Advances in scaling and modeling of land-atmosphere interactions

### Key Points:

- Adding containment lines into our wildfire model made the biggest difference in improving accuracy of daily burned area predictions
- Accounting for containment, fuel moisture content maps, and increased fuel density consistently increased prediction skill above persistence
- Modeled fire radiative power leads observations by at least an hour, but with similar accuracy to prescribed diurnal cycles

### Supporting Information:

Supporting Information may be found in the online version of this article.

### Correspondence to:

F. A. Turney,  
fturney@ucla.edu

### Citation:

Turney, F. A., Saide, P. E., Jimenez Munoz, P. A., Muñoz-Esparza, D., Hyer, E. J., Peterson, D. A., et al. (2023). Sensitivity of burned area and fire radiative power predictions to containment efforts, fuel density, and fuel moisture using WRF-fire. *Journal of Geophysical Research: Atmospheres*, 128, e2023JD038873. <https://doi.org/10.1029/2023JD038873>

Received 11 MAR 2023

Accepted 31 AUG 2023

### Author Contributions:

**Conceptualization:** Francis A. Turney, Pablo E. Saide









**Data curation:** Francis A. Turney, Pedro A. Jimenez Munoz, Xinxin Ye

**Formal analysis:** Francis A. Turney, Pablo E. Saide

© 2023. The Authors.

This is an open access article under the terms of the [Creative Commons Attribution License](https://creativecommons.org/licenses/by/4.0/), which permits use, distribution and reproduction in any medium, provided the original work is properly cited.

# Sensitivity of Burned Area and Fire Radiative Power Predictions to Containment Efforts, Fuel Density, and Fuel Moisture Using WRF-Fire

Francis A. Turney<sup>1</sup> , Pablo E. Saide<sup>1,2</sup> , Pedro A. Jimenez Munoz<sup>3</sup>, Domingo Muñoz-Esparza<sup>3</sup> , Edward J. Hyer<sup>4</sup> , David A. Peterson<sup>4</sup>, Maria E. Frediani<sup>3</sup>, Timothy W. Juliano<sup>3</sup> , Amy L. DeCastro<sup>3,5</sup>, Branko Kosović<sup>3</sup> , Xinxin Ye<sup>1,6</sup> , and Laura H. Thapa<sup>1</sup> 

<sup>1</sup>Department of Atmospheric and Oceanic Sciences, University of California, Los Angeles, Los Angeles, CA, USA, <sup>2</sup>Institute of the Environment and Sustainability, University of California, Los Angeles, Los Angeles, CA, USA, <sup>3</sup>Research Applications Laboratory, National Center for Atmospheric Research, Boulder, CO, USA, <sup>4</sup>Naval Research Laboratory, Monterey, CA, USA, <sup>5</sup>Department of Geography, University of Colorado Boulder, Boulder, CO, USA, <sup>6</sup>Institute of Urban Environment, Chinese Academy of Sciences, Xiamen, China

**Abstract** Predicting the evolution of burned area, smoke emissions, and energy release from wildfires is crucial to air quality forecasting and emergency response planning yet has long posed a significant scientific challenge. Here we compare predictions of burned area and fire radiative power from the coupled weather/fire-spread model WRF-Fire (Weather and Research Forecasting Tool with fire code), against simpler methods typically used in air quality forecasts. We choose the 2019 Williams Flats Fire as our test case due to a wealth of observations and ignite the fire on different days and under different configurations. Using a novel re-gridding scheme, we compare WRF-Fire's heat output to geostationary satellite data at 1-hr temporal resolution. We also evaluate WRF-Fire's time-resolved burned area against high-resolution imaging from the National Infrared Operations aircraft data. Results indicate that for this study, accounting for containment efforts in WRF-Fire simulations makes the biggest difference in achieving accurate results for daily burned area predictions. When incorporating novel containment line inputs, fuel density increases, and fuel moisture observations into the model, the error in average daily burned area is 30% lower than persistence forecasting over a 5-day forecast. Prescribed diurnal cycles and those resolved by WRF-Fire simulations show a phase offset of at least an hour ahead of observations, likely indicating the need for dynamic fuel moisture schemes. This work shows that with proper configuration and input data, coupled weather/fire-spread modeling has the potential to improve smoke emission forecasts.

**Plain Language Summary** Predicting wildfire growth and smoke behavior is an important and historically difficult task. Here we compare a coupled fire-weather model to current practices used in air quality forecasting in their ability to predict daily wildfire spread and fire intensity for the 2019 Williams Flats Fire. We also evaluate the fire-weather model against high-resolution satellite and aircraft measurements in ways previously unexplored. We find that including fire-fighting efforts in our model makes the biggest improvements toward accurate wildfire forecasting. When we account for fire-fighting efforts, fuel moisture maps, and increased fuel loads, our coupled fire-weather model significantly outperforms simpler methods with reasonable computational time. Despite this, modeled fire intensity tends to lead observations by at least an hour. Optimal configuration options and avenues for forecasting improvements are discussed.

## 1. Introduction

Large wildfires have become increasingly common in recent years (Abatzoglou & Williams, 2016) and their immediate destructive impacts are often followed by negative effects on regional air quality, public health, and the earth system. These problems have been exacerbated by the effects of climate change, historical containment efforts, and water usage, which have made fires more intense and more frequent, burning tree crowns more often and altering ecosystem succession dynamics (Halofsky et al., 2020). In turn, efforts to improve forest management, emergency response, and forecasting of air quality have the potential to reduce the negative impact of large wildfires on populations and the environment in a warming climate (McCaffrey et al., 2020). Air quality forecasting and emergency response efforts are commonly aided by models that predict wildfire growth despite considerable uncertainty associated with their configurations and inputs. Studies evaluating the accuracy and

**Funding acquisition:** Francis A. Turney, Pablo E. Saide

**Investigation:** Francis A. Turney

**Methodology:** Francis A. Turney, Pablo E. Saide, Pedro A. Jimenez Munoz, Domingo Muñoz-Esparza, Edward J. Hyer, David A. Peterson, Maria E. Frediani, Timothy W. Juliano, Amy L. DeCastro, Branko Kosović, Xinxin Ye

**Project Administration:** Francis A. Turney, Pablo E. Saide, Pedro A. Jimenez Munoz, Domingo Muñoz-Esparza

**Resources:** Francis A. Turney, Pablo E. Saide, Pedro A. Jimenez Munoz, Domingo Muñoz-Esparza, Maria E. Frediani, Timothy W. Juliano, Xinxin Ye, Laura H. Thapa

**Software:** Francis A. Turney, Pedro A. Jimenez Munoz, Domingo Muñoz-Esparza, Edward J. Hyer, Maria E. Frediani, Timothy W. Juliano, Amy L. DeCastro, Branko Kosović

**Supervision:** Pablo E. Saide, Pedro A. Jimenez Munoz, Domingo Muñoz-Esparza, Edward J. Hyer, David A. Peterson, Maria E. Frediani, Timothy W. Juliano, Branko Kosović, Xinxin Ye, Laura H. Thapa

**Validation:** Francis A. Turney, Edward J. Hyer, Xinxin Ye

**Visualization:** Francis A. Turney

**Writing – original draft:** Francis A. Turney

**Writing – review & editing:** Francis A. Turney, Pablo E. Saide, Pedro A. Jimenez Munoz, Domingo Muñoz-Esparza, Edward J. Hyer, David A. Peterson, Maria E. Frediani, Timothy W. Juliano, Amy L. DeCastro, Xinxin Ye, Laura H. Thapa

computational costs of wildfire models under different configurations can thus be crucial in informing communities in choosing modeling solutions.

Dynamic wildfire models come in a variety of architectures, but only a few direct comparison studies exist (Dobrinkova & Dobrinkov, 2014; Graff et al., 2020). These models generally fall into two classes, coupled or non-coupled, depending on whether heat from the wildfire influences the atmospheric flow or not (Bakhshaii & Johnson, 2019). Non-coupled models such as FARSITE (Finney, 1998), Prometheus (C. Tymstra et al., 2010), and BEHAVE (Andrews, 2014), are often used to aid firefighting efforts because of their computational speed and flexibility in inputting meteorological data from simulation or field, but these models are limited by their inability to resolve fire-weather interactions. Coupled models such as WRF-Fire (Coen et al., 2013), WRF-SFIRE (A. K. Kochanski et al., 2013), and CAWFE (Clark et al., 2004; Coen, 2005) are now widely used by researchers to better understand the mechanisms behind and interactions between wildfire spread, atmospheric turbulence, fire-weather, and smoke emission, but they are used less often for operational purposes because of longer computing times, complexity of configurations, and difficulty of validating the real-world outputs of these models. There have been recent efforts to gear coupled models toward operational forecasting (Jimenez et al., 2018; Kochanski et al., 2021; J. Mandel et al., 2014; Wang et al., 2022), but direct comparisons between coupled models and simpler approaches are rare in the scientific literature (Dobrinkova & Dobrinkov, 2014; Wang et al., 2022). Additionally, multiple studies have been performed to assess the sensitivity of fire-spread modeling to a variety of factors including fuel moisture representation (Matt Jolly, 2007), ignition location and timing (Zinger et al., 2020) and ignition ahead of the fire line by spotting (Frediani et al., 2021). However, we are not aware of work exploring observed containment efforts in the context of coupled fire-weather modeling, and more realistic treatments of heat release due to canopy burning are underway (Shamsaei et al., 2023).

Despite the widely understood interactions between fire and local weather, operational air quality forecast models still often rely on “persistence forecasting,” in which daily burned area from the previous day is assumed to repeat and thus forecast emissions on the subsequent days (Ye et al., 2021). Persistence forecasts fail to account for the dynamic nature of wildfires, and their performance will be especially poor on days of large fire growth or decline (Ye et al., 2021). Although several tools have been explored to overcome the deficiencies of persistence forecasting (Graff et al., 2020; Peterson, Hyer, et al., 2013; Peterson, Wang, et al., 2013; Preisler & Westerling, 2007), persistence forecasting remains a de facto standard for smoke forecasting models. Along with persistence in burned area, Fire Radiative Power (FRP), or the radiant energy released by a fire, is also predicted as a function of the previous days burned area in models such as HRRR-Smoke (Ahmadov et al., 2017) and NCAR WRF-CHEM (Kumar et al., 2021). FRP has been found to be highly correlated with smoke emissions from wildfires (Wiggins et al., 2020), and important to modeling smoke injection heights (Ye et al., 2021), thus making another great benchmark for WRF-Fire comparisons.

Here we evaluate a case-study set of simulations produced by the coupled fire-spread model WRF-Fire (Coen et al., 2013; J. Mandel et al., 2011; Muñoz-Esparza et al., 2018) to better understand the potential of coupled models to predict daily burned area and FRP. Persistence and smoke emission models are used as benchmarks and configurations are varied within the set to reflect potential operational considerations. WRF-Fire can capture realistic fire growth, regional meteorology, and Large Eddy Simulation (LES) scale fire induced weather patterns all at once with potentially reasonable computing time, making it a prime candidate for improvement over simpler methods.

We focus this study on the 2019 Williams Flats Fire, as it was the most intense fire sampled during the 2019 NASA/NOAA Fire Influence on Regional to Global Environments and Air Quality (FIREX-AQ) field campaign. The Williams Flats Fire was ignited by lightning and fuel-driven for the first few days before exploding in growth after the breakdown of an upper-level high pressure ridge and subsequent period of enhanced wind speeds and instability (Peterson et al., 2022). There were significant efforts to contain the fire and protect surrounding buildings which seem to have succeeded in cutting the fire off in the southern and western flank. In addition, a pyrocumulonimbus (pyroCb) cloud developed during the final days of the fire (Peterson et al., 2022). We perform WRF-Fire simulations starting from both a point source representing ignition, as well as from perimeter observations. Simulations are run for multiple days, and initialization at different days is compared. We then analyze WRF-Fire's forecasting skill under a variety of sensitivities that the end user has control over including horizontal resolution, fuel moisture, fuel density, ignition method, and inclusion of containment data.

## 2. Methods

The methods are divided into groups either describing WRF-Fire (Section 2.1 – 2.4) or comparisons with other models and observations (Section 2.5). We discuss WRF's background, meteorological forcing, and resolution in Section 2.1, input data and preprocessing in Section 2.2, and fire-code implementation in Section 2.3. Our configuration choices and motivations are detailed in Section 2.4 before discussing comparisons to observations and benchmarks in Section 2.5.

### 2.1. Weather Model (WRF)

All of our simulations have WRF (Weather Research and Forecasting tool) at their core (Skamarock et al., 2019), a long-standing community model capable of simulating a wide range of atmospheric phenomena from global climate to cloud microphysics. We take advantage of WRF's nested domain configuration options, to feed synoptic meteorological data through a coarse-resolution domain and into a high-resolution LES domain where the fire code runs. This form of mesh refinement is a common practice in WRF and allows us to resolve several scales of meteorology at once.

Our WRF simulations use a two-domain configuration going from 1-km resolution on the outer domain to 200 m on the inner domain; we include only one way coupling from the outer to the inner domain. Using a 50 km by 50 km inner domain and 200 km by 200 km outer domain, together with the meteorological boundary conditions from 3 km HRRR forecasts, WRF can resolve synoptic, mesoscale, and boundary layer features for many days into the simulation. Mesoscale/synoptic meteorology is a well-known driver of wildfire behavior, with surface wind events commonly linked to the breakdown of the upper-level ridge or passing of synoptic lows and fronts (Tymstra et al., 2021).

We choose 200 m for the base LES horizontal resolution because at the scale of medium-large wildfires (~50 k acres), it allows us to run two to three times as fast as reality. Although 200 m is in the gray zone (aka terra incognita), or the range at which PBL schemes and LES can both underperform (Juliano et al., 2022; Rai et al., 2019; Wyngaard, 2004), our early results indicated that increasing the resolution to 100 m grid spacing did not improve simulations significantly enough to warrant the extra computational time (see Figures S1 and S2 in Supporting Information S1).

It's well known that turbulence plays a significant role in the way weather and wildfire activity interact (Section S1 in Supporting Information S1). Here we simulate some of those important dynamics through WRF's LES configuration. In our inner domain, the Planetary Boundary Layer (PBL) scheme is turned off and a 3D turbulent kinetic energy (TKE)-based sub-grid scale (SGS) scheme is used to predict eddy diffusivity (Deardorff, 1980).

### 2.2. Input Data (WPS)

For all simulations, we use the WRF Pre-processing System (WPS) to interpolate input data and format the data to be read by WRF. Both domains require interpolation of meteorological data, topography, and land-surface data, while data such as fuel category, fuel density, and fuel moisture are interpreted to the fire model sub-grid.

Our simulations run with initial and boundary conditions from the High-Resolution Rapid Refresh (HRRR) model, which are 3 km resolution hourly updated instances of WRF from NOAA that run over the United States (Benjamin et al., 2016). HRRR assimilates data from satellite, aircraft, and many other observations and is forecasted out up to 48 hr in advance at every six-hour forecast, and 18 hr in advance otherwise. Here we always use the 0-hr forecast for initial and boundary conditions which are the closest to observation. Although there are other meteorological products with similar resolutions that would be suitable for WRF-Fire (NAM 3 KM CONUS) we are not aware of a public archive for them, and other meteorological forecasting data available are too coarse to use in a single nested domain study. The impact of using either coarser or non-archived meteorological input data is left to future studies.

While our outer domain uses default topography to simulate mesoscale phenomena, turbulence in an LES domain needs a roughness element or initial disturbance to be spun up realistically. A fully spun up Atmospheric Boundary Layer (ABL) may require long fetches over steep topography or continuous perturbation methods (Lee et al., 2019) so to trip turbulence here, we use high-resolution topography and a roughly 20 km fetch

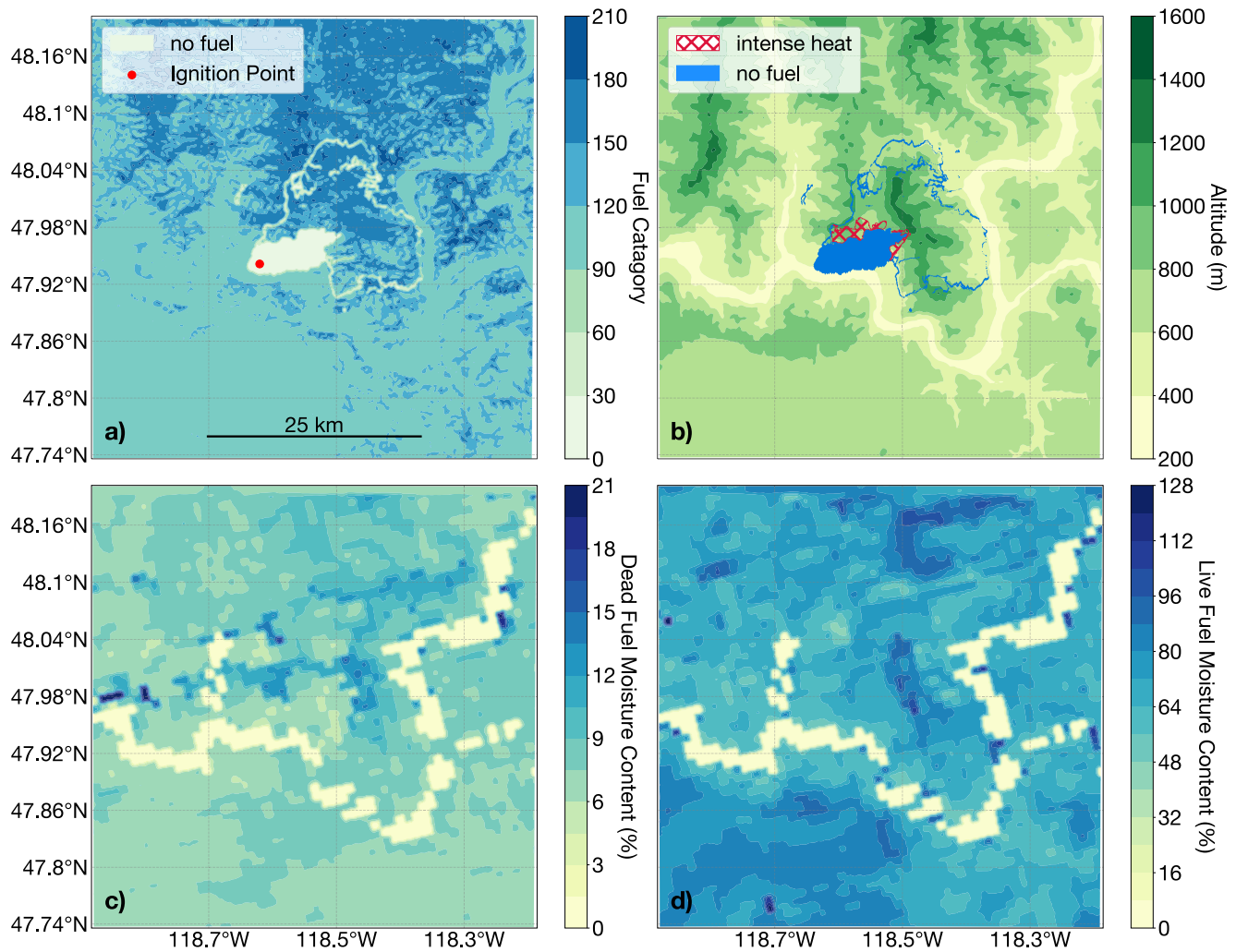


**Figure 1.** Inputs for WRF-Fire simulations of the 2019 Williams Flats Fire ignited just before August 4th. (a), fuel categories represented here include dry grass (102), dry timber-shrub (165), long-needle litter (188), and no fuel (14, light green, see Section 2.3) from the 40-category data set (Scott, 2005). Ignition point is chosen as approximately the middle of the first VIIRS retrieval (see Figure 2). (b), No-fuel sections of fuel category are either the scattered and no heat areas at the interior of the fire or containment lines. The intense heat region in hatched red, taken from NIROPS the night of August 3rd, is the only region which is set to burn at the start of simulation.

in all directions. Although confirmation of fully developed turbulence is beyond the scope of this study, key turbulent structures and interactions appear in our simulations (Section S1 and Figures S3–S5 in Supporting Information S1).

Our 30 m resolution topographic data set comes from the LANDFIRE archive (Landscape Fire and Resource Management Planning Tools, (Ryan & Opperman, 2013)) where data is available over the contiguous United States (Figure 1). The 30 m topographic data is interpolated to the 200 m LES grid and either smoothed slightly using the WPS native smoothing found in *GEOGRID.TBL* or spectrally smoothed (Kosovic, 2021) to obtain speed-ups for possible operational purposes. Smoother terrain lowers vertical wind velocities and reduces the chance of winds being advected beyond a cell's length (De Moura & Kubrusly, 2013). This allows for numerical stability on larger time steps and computational speeds of up to six times faster than reality for this fire (Section 2.4).

Another consideration in modeling with WRF is the use of land-surface models. We selected the highest resolution land cover data set intrinsic to the general WRF static input data, a 9 s NLCD (National Land Cover Database) data set, which is specified during the pre-processing configuration, on the *namelist.wps* file:

```
geog_data_res = 'nlcd2006_9s + 30s','3s + nlcd2006_9s + 30s'
```

Fuel category is central to WRF-Fire's burning scheme in separating types of fuels and their propensity to burn and spread. We gather fuel category data from the LANDFIRE website (Ryan & Opperman, 2013), which uses the Fuel Characteristic Classification System (FCCS) and separates fuel loads into low, medium, or high load categories. We performed our simulations using the 2016 version of the FCCS classification using either the 13-category (Anderson, 1981) or 40-category data (Scott, 2005). A number of corresponding coefficients that influence fire-spread are listed in the configuration file *namelist.fire* (see Data Availability Statement), including fuel density, fuel depth, and weighting coefficients for mass loss rate curves.

Dry fuels can be a significant driver of wildfire behavior and smoke emission, and to better understand model sensitivity to fuel moisture, we incorporate recently derived fuel moisture satellite products into WRF-Fire as static input conditions (Kosović et al., 2020). Here we use the WRF-Fire code developed for Colorado Fire Prediction System (CO-FPS) which allows fuel moisture content (FMC) maps from the Moderate Resolution Imaging Spectroradiometer (MODIS) instruments Terra and Aqua to be ingested into our simulations at 1 km resolution (Kosović et al., 2020). Fuel moisture maps (Figures 1c and 1d) are static for each simulation and are usually retrieved around 12 hr before the start of our fire simulations. There are dead and live fuel moisture maps, and in the CO-FPS model live fuel can both burn and be converted to dead fuel. The dead FMC maps that we use are typically lower in FMC (6.5% mean value for Figure 1c than what WRF prescribes as its default value (8%)) and as dead fuels make up the bulk of the fire-spread along the ground, we generally get faster fire spreads when using these satellite FMC products as inputs.

### 2.3. Fire-Spread Model (WRF-Fire)

At the smallest scales of our simulations is the fire-spread model, a sub-grid semi-empirical algorithm with the Rothermel equations at its core (Rothermel, 1972). Like many other fire-spread models the rate-of-spread (ROS) is a function of wind speed, fuel moisture, and slope of the topography with scaling effects from fuel properties. Fuel combustion rate scaling factors set in the configuration file *namelist.fire* modulate these equations and thus influence the ROS and heat release of the model. Inputs are interpolated, combustion is parameterized, and the fire front is propagated on our LES domain's sub-grid with a grid spacing of 50 m (Coen et al., 2013).

The propagating fire line is tracked by an improved level-set function which represents a line as the intersection of a signed three-dimensional curve and a plane (Muñoz-Esparza et al., 2018). This allows for fire lines to split and rejoin in natural ways and is generally considered more accurate than other common methods for representing fire line such as Huygen's elliptical algorithm (Anderson et al., 1982). The signed nature of the curve, negative on the inside of the fire, is a crucial part of propagation, but over time the function can accumulate error, lose its signed nature, and yield inaccurate results (Chopp, 1991; Sussman et al., 1994). A reinitialization of the level-set function is often implemented to account for this and the number of iterations of the algorithm can thus act as an important numerical parameter. WRF-Fire recently received an update implementing high-order numerical methods to advance the level-set function and re-initialization as part of the fire-spread model (Muñoz-Esparza et al., 2018) which we use in this work. A dependence of the re-initialization on the LES time step was discovered in this work and changes were made to the "FIRE\_LSM\_REINIT\_ITER" parameter to account for this (Section S2 in Supporting Information S1). For this study, we find 3.3 iterations of re-initialization per second to be optimal.

WRF-Fire can be ignited by points or lines but over time may deviate significantly from observation. In addition, after a long integration (~>2 days) it becomes impractical to start from point ignitions. To overcome this, WRF-Fire can also be ignited from an observed perimeter, which can help realign a simulation with observations and reduce the computational time compared to simulating the fire progression from a point/line. Here we use the National Infrared Operations (NIROPS) aircraft retrievals, flown at most once a day on large wildfires, which have high spatial resolution and resolve regions of high intensity, scattered heat, and no heat. Within the fire perimeter, negative values are written into WRF's Level-Set Function (LSF) history variable to represent burning regions. In the scattered and no heat regions within the perimeter, we remove the fuel so that no burning over already burnt fuels occurs.

Currently, WRF-Fire only considers the burning of surface fuels and thus can underpredict heat flux where crown fires have occurred. Here we implement a modification of fuel densities ( $\text{kg/m}^2$ ) to make up for the missing fuel

**Table 1**  
*Simulation Configurations*

|             | 200 m<br>topo | 275<br>smooth<br>topo | Fuel<br>moisture | Fuel<br>density<br>scaling | Containment |
|-------------|---------------|-----------------------|------------------|----------------------------|-------------|
| Base        | ✓             |                       |                  |                            |             |
| Crown       | ✓             |                       |                  | ✓                          |             |
| FMC         | ✓             |                       | ✓                | ✓                          |             |
| Smooth-FMC  |               | ✓                     | ✓                | ✓                          |             |
| Contain-FMC | ✓             |                       | ✓                | ✓                          | ✓           |
| Contain     | ✓             |                       |                  | ✓                          | ✓           |

*Note.* Differences between simulations' configuration options with check marks indicating which features (columns) and used in which configurations (rows). Topo is short for topography, and explanations for configuration options are described in Section 2.4.

load and subsequent heat output when burnt. For the 13-category fuel category data, we replace fuel densities with their closest corresponding category value from a list of average fuel densities for wildfires over three major fuel types in FINN (Fire INventory from NCAR, (Wiedinmyer et al., 2011) corresponding to grasslands (0.98 kg/m<sup>2</sup>), savannah (5.7 kg/m<sup>2</sup>) and temperate forest (10.49 kg/m<sup>2</sup>). Other fuel loading models and observations in the region show a wide range of estimates with FINN values falling in between and getting closer to observations than most (Drury et al., 2014). In addition, the data from FINN represents average fuel densities burned for different fuel categories, which includes canopy burning, making it an ideal choice for an implicit model which aims to correct fuel density burning on average rather than explicitly accounting for canopy fires. For the 41 category fuel category data, we group the categories into the three major FINN categories and then normalize their fuel density, so the average of the group is equal to the corresponding FINN value, thus retaining the relative variability for categories within each group (Figure 1; Table S1 in Supporting Information S1). Both methods yield significant improvements in heat output when compared to satellite retrieved FRP (Section 3.3). A caveat of this implementation is that it assumes all fuel is on the surface and thus could affect fire spread. However, we kept this implementation as this sensitivity has not been assessed in previous work and it allowed for increased heat release without having to develop a canopy burning parameterization.

The National Interagency Fire Center (NIFC) has a repository through ArcGIS online for historical wildfire containment data that we use in this work. Here we take completed containment lines from the “EventLine2019” operational data archive and filter them to keep completed dozer lines, completed hand lines, completed lines, and roads as completed lines for the Williams Flats Fire. The dates of completion for the containment lines appear to be inaccurate or incomplete at this time, as many lines are listed as being completed well after the fire burned past them. Handwritten notes on the efforts exist but to our knowledge are only available to fire crew. With that in mind, we use this data in an ideal sense, removing fuel along every containment line available for the fire from the very beginning as if all containment lines were constructed before the fire reached them (Figures 1a and 1b). This assumption is likely valid given that crews would not complete a line after a fire burned past. We additionally compared containment lines to road maps and found most lines are on roads, possibly indicating that lines were established well ahead of time. However, using containment lines with accurate dates would possibly yield different simulation results, likely burning past final containment perimeters more when simulations overestimate fire spread. At this time, we are not aware of real-time data available for such containment efforts so simulations that use this method are only meant to show the difference that modeling containment could make in WRF-Fire in a best-case scenario.

#### 2.4. Model Configurations Tested

Because there were so many variables affecting fire-spread in any given simulation, we selected a few key configurations from the above-mentioned methods to test the model's sensitivity to important factors by sequentially increasing the realism of the simulations. We tested 6 different configurations: Base, Crown, FMC, Smooth-FMC, Contain-FMC and Contain (Table 1). All simulations share outer domain settings, domain boundaries, sub-grid turbulence parameterizations, standard meteorology schemes, HRRR input meteorology, and 9 s land category data. We take as *Base* simulation what we consider to be closer to default settings, 200 m horizontal resolution, 13-category fuel data, and homogenous fuel moisture supplied in the default version of *namelist.fire* of 0.08 kg/kg. To represent a fire that has crown burning, we alter the base simulation by scaling up the 13-category fuel density (Section 2.3; Table S1 in Supporting Information S1) in *Crown* simulations. We add FMC maps from NCAR for a *FMC* simulation, although we also use scaled 41-category fuel category data to match developer configurations and capture the most accurate representation of heat release (Section 2.2; Table S1 in Supporting Information S1). For a less computationally intensive model we alter the Fuel Moisture simulation by spectrally smoothing topography to 275 m (Section 2.2) which we label *Smooth-FMC*. In our *Contain-FMC* sensitivity, the FMC simulation is used but all the fuel category cells overlapping with containment lines from containment lines

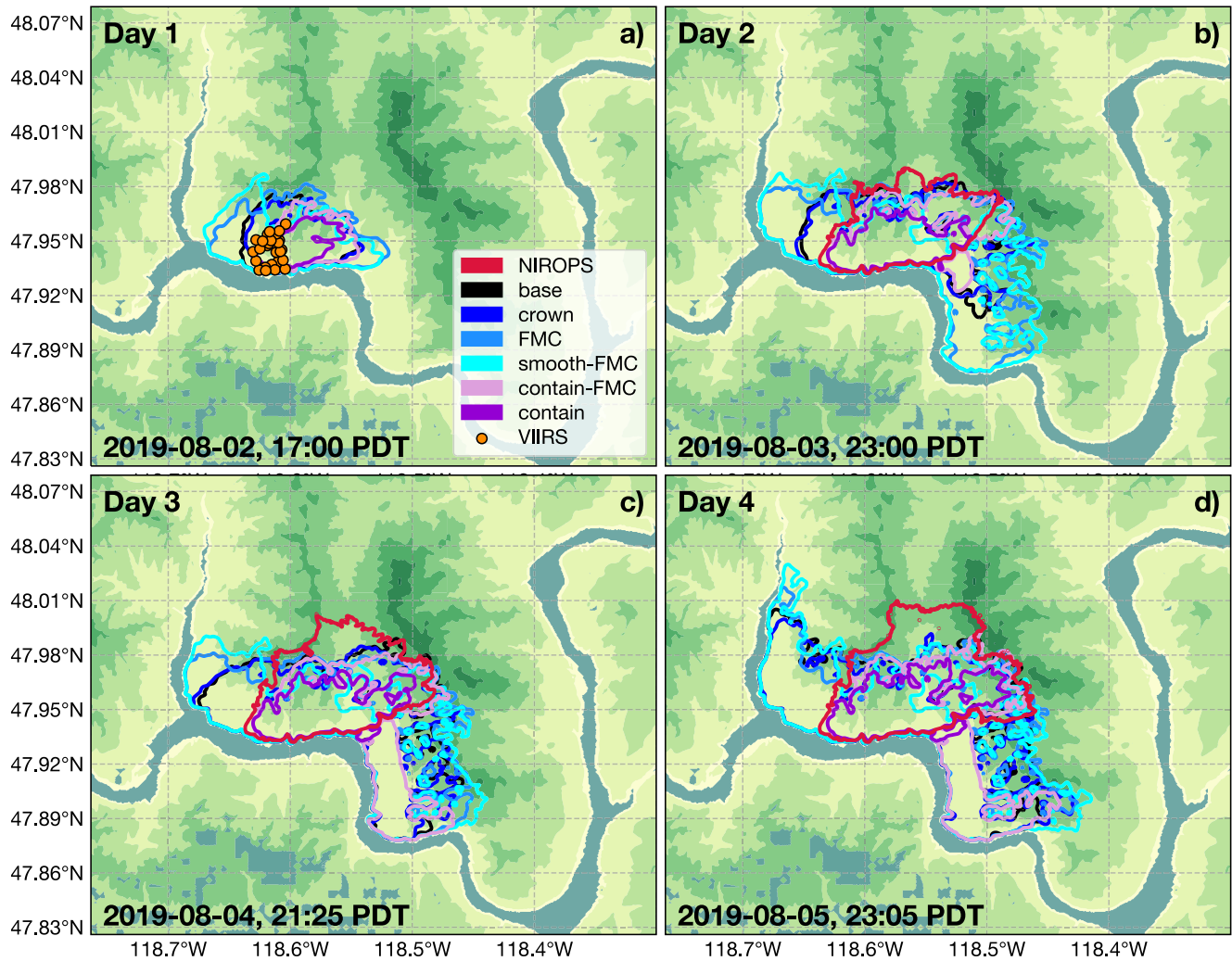


**Figure 2.** The first 4 days of point ignited simulations for the 2019 Williams Flats Fire. For a breakdown of sensitivities see Section 2.4 and/or Table 1. VIIRS hot spots are 375 m resolution satellite products that indicate the presence of fire and pass near any location usually twice per day. The simulations were ignited at 3 a.m. PDT, near the time of first report, at the ignition point shown in Figure 1.

are set to the zero-fuel category to simulate an ideal containment scenario (Section 2.3). Our final sensitivity *Contain* takes the contain simulation and turns off the fuel moisture scheme so we can analyze the effect of our ideal containment scenario without FMC. We also construct an *Ensemble* average forecast from the FMC and Crown sensitivities as they are usually the furthest spread apart in predictions and feasible for use in an operational setting.

### 2.5. Observations and Benchmarks

Active fire products from NOAA's Geostationary Operational Environmental Satellites (GOES) Advanced Baseline Imager (ABI) produce fire count and Fire Radiative Power (FRP) at 5-min intervals using the Wildfire Automated Biomass Burning Algorithm (WFABBA) algorithm (Schmidt, 2020). These GOES-17 fire pixels were filtered similarly as in previous work (Li et al., 2022) based on flag and only kept if the flag was for a processed fire pixel (10), high-probability fire pixel (13), or medium probability fire pixel (14) excluding cloudy, saturated, and low probability fire pixels. GOES data was not parallax corrected, but aggregated over a box where pixels corresponding to the Williams Flats fire are still contained (Lat 47.90–48.05, Lon –118.67–118.3) as done in previous work (Ye et al., 2021; Berman et al., 2021). Here we use data from GOES-17 to evaluate wildfire simulations at higher-temporal resolution than any comparison that we are aware of in the literature. To directly compare WRF-Fire and GOES-17 FRP, WRF-Fire output is re-gridded to the GOES-17 grid by summing up heat fluxes inside GOES-17 cells (2 km

horizontal resolution). Comparing cells that are on fire in WRF-Fire versus GOES-17 on the GOES-17 grid gives us a unique comparison in fire count, which is the number of pixels deemed on fire by GOES-17 or assumed on fire if GOES-17 could somehow observe our simulation (i.e., Equivalent Fire Counts). In addition, summing up the total radiant power over all cells inside the fire domain (calculation described below) gives us a measure of a simulated fire's FRP. Both FRP and Fire Count are processed on 5-min windows and then averaged over each hour.

These comparisons rely on a few assumptions about the amount of radiation from the fire that would realistically be observed by GOES-17. First, we assume that only 20.5% of the total heat released by WRF-Fire (Sensible + Latent) is in the form of radiation that can be observed by satellite. This ratio is an average of the ideal range of radiant fraction measured in Johnston et al. (2017), which is notably at the higher range of estimates compared to previous studies (Freeborn et al., 2008) but not outside classical estimates (Byram, 1959). The rest of the heat is assumed to be partitioned into latent, convective, and conductive heat. In reality, the exact ratio is likely more variable and dependent on at least sensor angle (Johnston et al., 2017), wind speed, fuel depth, fuel moisture, and fuel category (Frankman et al., 2012), but we use a constant given the considerable uncertainty in those relationships in the literature. Second, we assume that GOES-17 has a minimum FRP per pixel that it can detect, below which the pixel will not be considered on fire. We take this minimum value to be 25 MW per pixel based on the similar resolution between GOES-17 and MODIS Aqua's day edge, where the exponential drop off in FRP density is around 25 MW (Peterson, Hyer, et al., 2013; Peterson, Wang, et al., 2013). More recent studies (Li et al., 2020; Xu et al., 2021) found thresholds of 30–35 MW for GOES retrievals, but differences in FRP and Fire-count were nearly imperceptible across this range. A snapshot of WRF-Fire's equivalent fire counts versus GOES-17's fire counts shows that the algorithm produces a realistic pixel distribution (Figure S7 in Supporting Information S1). In addition, while fire counts shown in Figure 8 show reasonable agreement after thresholding, choosing a minimum pixel power threshold was found to not significantly affect FRP results.

We used several other data sets to evaluate WRF-Fire against. The Visible Infrared Imaging Radiometer Suite (VIIRS) is a sensor on board the S-NPP satellite that usually samples fires twice a day (day and night overpasses), and produces fire hotspot pixels and FRP at a nadir resolution of 375 m (Schroeder & Giglio, 2017). Fire hotspots were aggregated to estimate burned area (Berman et al., 2021) which we use in cases of missing NIROPS flights along with a VIIRS FRP product that was used to evaluate WRF-Fire equivalent FRP. We also compared WRF-Fire FRP to the MODIS/ASTER Airborne Simulator (MASTER), an infrared sensor flown on the DC-8 aircraft during FIREX-AQ from which an FRP estimate can be derived as done in previous work (Thapa et al., 2022).

Assumptions commonly used in smoke forecasting are used here as benchmarking metrics. We compare WRF-Fire predictions of daily burned area to a persistence forecast computed using the difference between NIROPS perimeters on Day 0 and the previous day. When NIROPS is not available we used a VIIRS based estimate (Berman et al., 2021). HRRR-Smoke (Ahmadov et al., 2017) and NCAR WRF-CHEM (Kumar et al., 2021) are smoke forecasting models which have fixed diurnal cycles that we compare WRF-Fire diurnal activity to. The diurnal cycles are normalized by the magnitude of the sum of FRP values (Ye et al., 2019, 2021).

Although there are no high-quality observations of surface meteorological conditions within our second domain, comparisons between nearby US Forest Service Remote Automatic Weather Stations (RAWS) and WRF meteorological variables provided us some insight into our simulations accuracy in simulating the weather events that influenced the Williams Flats Fire. The Wellpint RAWs stations is ~35 km from the Williams Flats Fire so it provides basic meteorological diagnostics for the region. Figures S8 and S9 in Supporting Information S1 show the timing and magnitude of WRF winds are likely reasonable although perhaps slightly underpredicted. Air temperature and Relative Humidity (RH) also show reasonable magnitude and temporal cycles. Although only one WRF-Fire simulation is shown, it's representative of the other simulations and days.

Computational times over this 50 km × 50 km domain with 400 cores were six times faster than reality when spectrally smoothed, and three times faster otherwise, but consistent results depend on adjusting the number of re-initialization iterations if the time step is reduced.

### 3. Results

#### 3.1. Burned Area Perimeters

Burned area perimeters are plotted for our simulations at times corresponding to NIROPS perimeter products or VIIRS retrievals (Figures 2 and 3; Figure S11 in Supporting Information S1). We find that, especially in point-ignited simulations, spatial differences between WRF-Fire and NIROPS's burned area perimeters generally increase over time



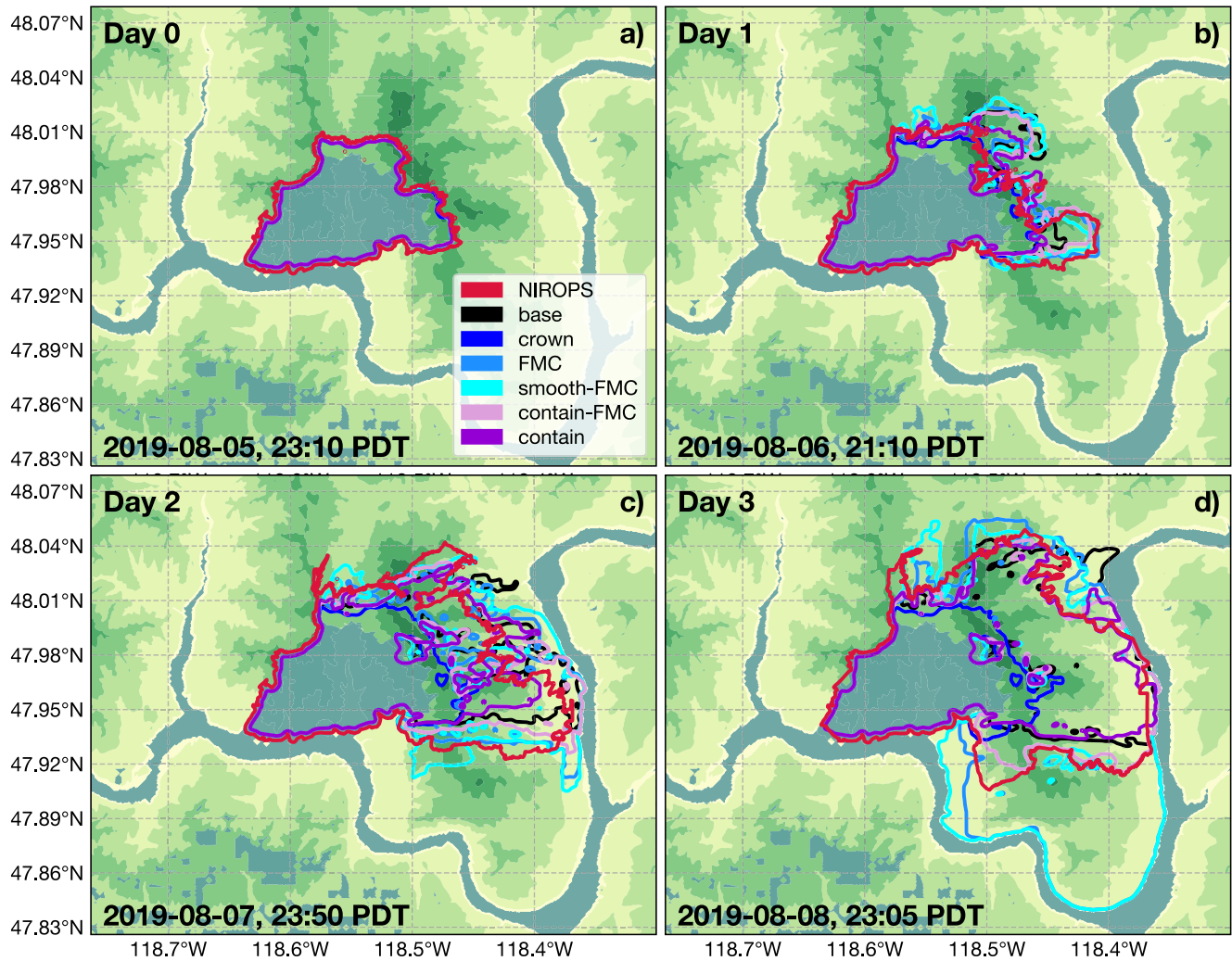


**Figure 3.** Three-day forecasts of WRF-Fire's real perimeter ignition simulations, starting at 23:10 PDT on 5 August 2019, for the Williams Flats Fire. See Section 2.4 and/or Table 1 for a breakdown of different simulations. The gray blue color of the river that also extends into the center of the fire is the no-fuel region, here representing burnt out fire interiors, water, and urban or agricultural non-fuels.

as we might expect from a stochastic weather forecast (Figure 2). As time passes, errors compounded on each other, with fires continuously spreading along fronts that were contained (Figure 1b) or continuously stagnating in directions that should have burned more quickly (Figure 2). Simulations often burned too much along the grassy southern and western flanks where containment was effective and not enough into the forested mountains where containment lines were sparse (Figure 1b). Inclusion of containment lines yielded better perimeters in almost all cases, although in the case of a point ignition the fire seemed to make its way through the containment perimeter, likely either because of gap in containment data or a river that is not well represented in the fuel category data (Figure 2).

When igniting WRF-Fire from an observed fire perimeter (i.e., later into the fire), many of these problems were minimized (Figure 3). Often, the already burned interiors blocked fire from spreading back into already burned areas, forcing spread in the right direction. Also, because the fire burn toward a large river bend in the south and east, simulations ignited or burning later into the fire were trapped within these natural boundaries.

### 3.2. Total Burned Area and Daily Burned Area

From these perimeters we calculate a total burned area time series for WRF-Fire simulations to compare against observed burned area estimates (Figures 4a and 5a). We found the most consistent way of computing burned area from WRF-Fire was to input the wildfire perimeters from our spatial plots (e.g., Figures 2 and 3) into a polygon area calculation scheme using an equal area projection (see Data Availability Statement). Differences in initial

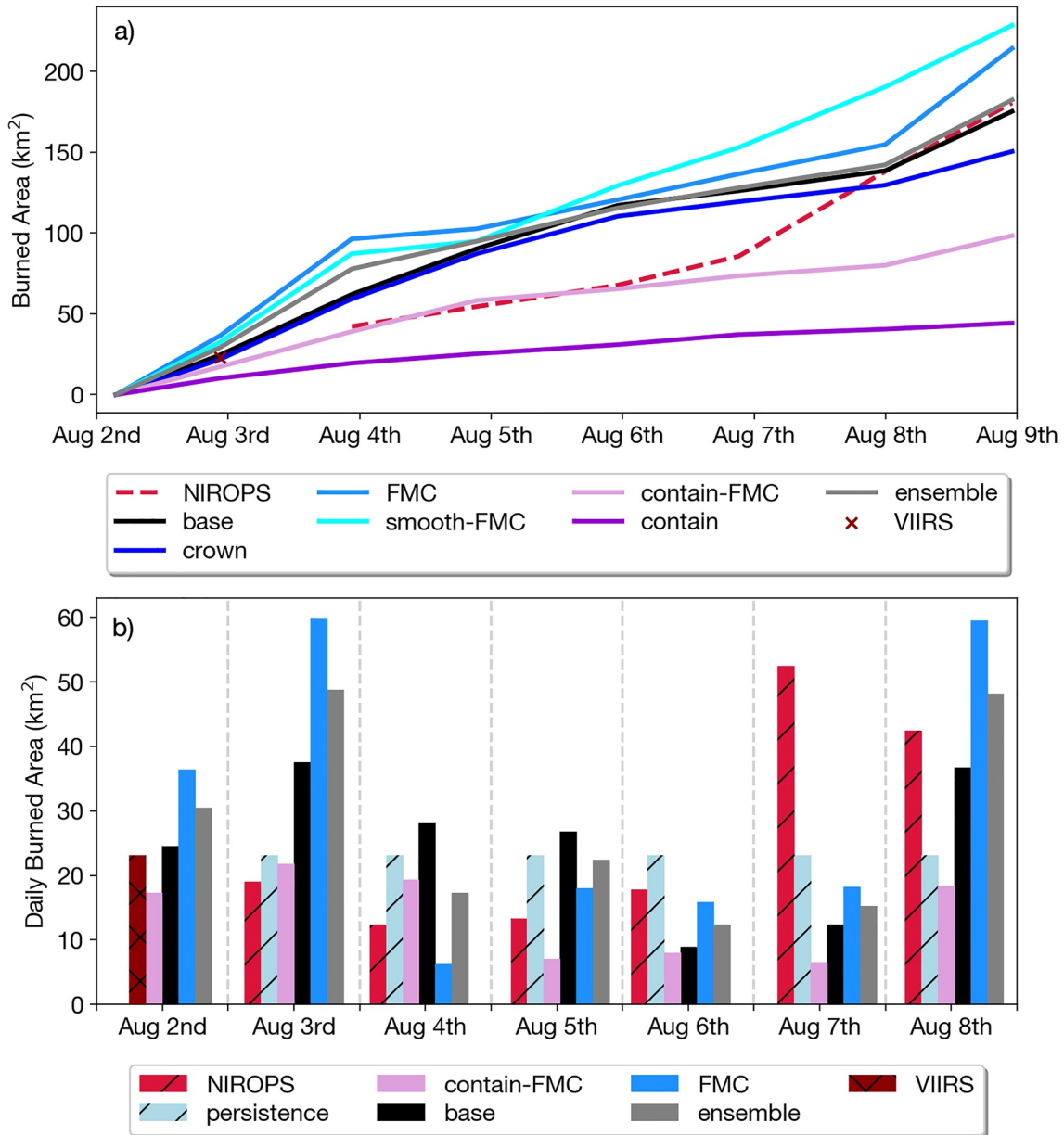


**Figure 4.** (a), Time series of total burned area for point ignited simulations. See Section 2.4 and/or Table 1 for a breakdown of different simulations. (b), Daily burned area for the same set of simulations and observations as (a). Persistence is forecasted for 6 days and based on the day 1 VIIRS burned area estimate.

burned area between NIROPS and WRF-Fire when starting the fire from a real perimeter (e.g., 23 PT on August 5th in Figures 3 and 5) can be attributed to the way the level-set function is written into the inputs as a distance transform that results in slightly positive values close to and inside the perimeter. This is likely a relatively small factor in the prediction skill overall.

NIROPS perimeters are taken once every night, if flight conditions are favorable, when the fire has mostly finished burning, so we take differences in consecutive NIROPS perimeters as daily burned area observations. We also take differences in WRF-Fire perimeters over NIROPS retrieval windows when calculating daily burned area for WRF-Fire (Figures 4b and 5b). Using the Root Mean Squared Error (RMSE) between daily burned area predictions and NIROPS observations we calculate and plot the Skill Score as defined by:

$$\text{Skill Score} = 1 - \frac{\text{RMSE}(\text{WRF})}{\text{RMSE}(\text{persistence})} \quad (1)$$

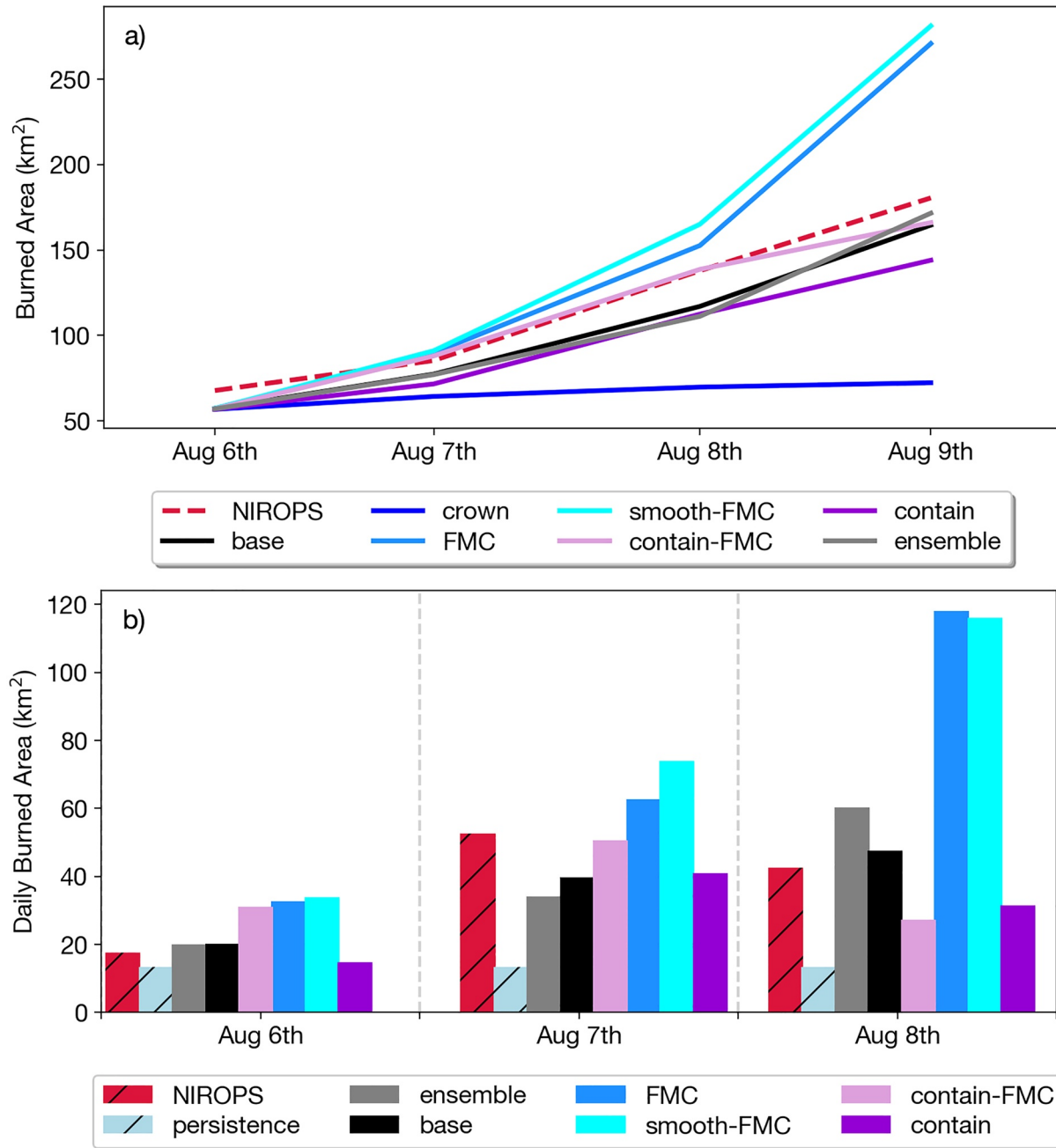


**Figure 5.** (a), Burned area time series for real perimeter ignited simulations starting on 6 August 2019. See Section 2.4 and/or Table 1 for a breakdown of different simulations. (b), Corresponding daily burned area plot.

The skill score is computed for all simulation days and sensitivities (Figure 6), positive values representing fractional improvement over persistence and 0 or below indicating reduced skill. Because this is a single fire with just five different ignition days, data quantity and therefore generalizations are limited, but the trends appear consistent and explainable for this study.

In general, we see a significant overestimation of burned area in our time series unless fuel density was increased or containment modeling was used (Figures 4 and 5). We note that simulations without containment at times bound the observations (Figure 5; Figure S14 in Supporting Information S1) and thus their ensemble average has the potential to predict burned area progression better than those individual models. Here we took the *ensemble* product to be the average of the *crown* and *FMC* configurations because they often display opposite behaviors,

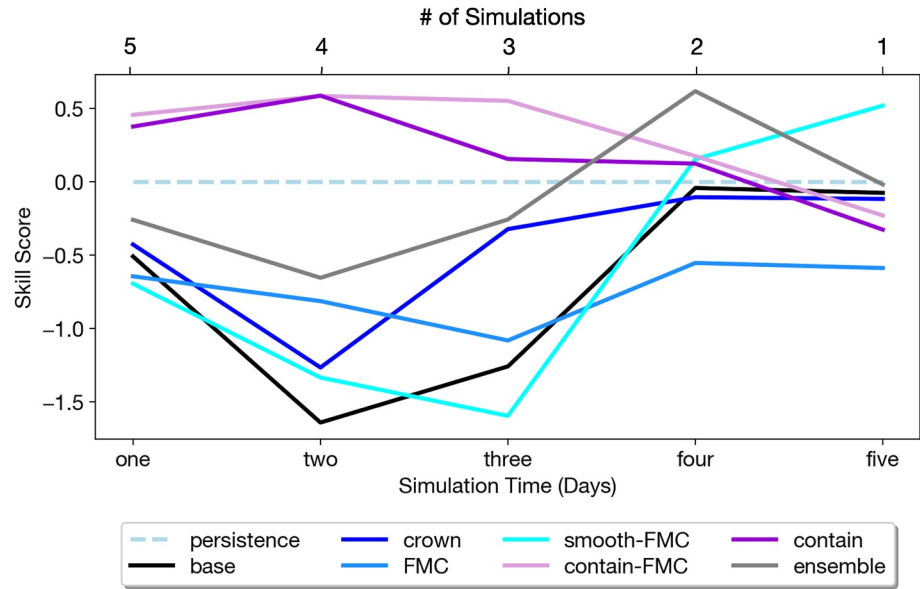


**Figure 6.** Time series of Skill Score (Equation 1) between WRF-Fire and NIOPS on daily area burned. Positive values represent fractional improvement over persistence, zero or negative values indicate reduced or no skill increase. Top axis shows the number of simulations per data point. There were 5 one-day forecasts, 4 two-day forecasts, 3 three-day forecasts, 2 four-day forecasts, and 1 five-day forecast. The same breakdown goes for persistence forecasts.

underestimating and overestimating respectively. Including only two models in the ensemble average also allows for the potential for reasonable computational time of the average in an operational setting. We find that on average, the ensemble forecast outperforms all other non-containment configurations in predicting daily burned area (Figure 6).

We find that simulations which consider containment modeling (*contain*, *contain-FMC*) have higher skill than persistence for the first few forecast days, but which decreases over time (Figure 6). Predictions of daily burned area in our *contain-FMC* simulations are, on average, 30% more accurate than persistence over a 5-day forecast. In contrast, simulations without containment show a steep skill decrease on days one and two followed by an increase on later days, in some cases becoming more skillful than persistence toward the end of the fire. We can also see that using containment modeling together with fuel moisture maps yields better results than the containment measures alone, on average 15% more accurate in daily area burned over a 5-day forecast. Including fuel moisture maps, without containment modeling, did not improve our accuracy overall but *FMC* runs did add to skill when used as a factor in the ensemble average values. Despite topography being spectrally smoothed to 275 m, *smooth-FMC* configurations do not show a large decrease in skill compared to other non-containment models in our results.

We also plot the absolute error in daily burned area for one, two, and 3-day forecasts versus their ignition day (Figure 7). In the *ensemble* average and in models without containment, we can see that accuracy improves as perimeters are ignited later in time, at times improving upon persistence for day one forecasts when ignited on later days. This is likely to be a result of the fire being trapped between the river and its own burnt-out interior on later fire days as described in Section 3.1, although other factors are expanded on in the discussion.

### 3.3. Evaluation of Energy Release and Diurnal Cycles

We produce an FRP and fire count product (Section 2.5) from WRF-Fire and show one of our more accurate ignition days simulations (Figure 8). Fire count curves have similar magnitude and shape to GOES-17 products, suggesting that our physical thresholding, radiant heat fraction, and re-gridding process allows for a reliable comparison framework between WRF-Fire heat outputs and GOES-17 FRP retrievals.

We find that for configurations that have scaled fuel density, FRP values are always closer to observation on 1-day forecasts and usually closer to observation in following days, alluding to the lack of canopy burning in WRF-Fire

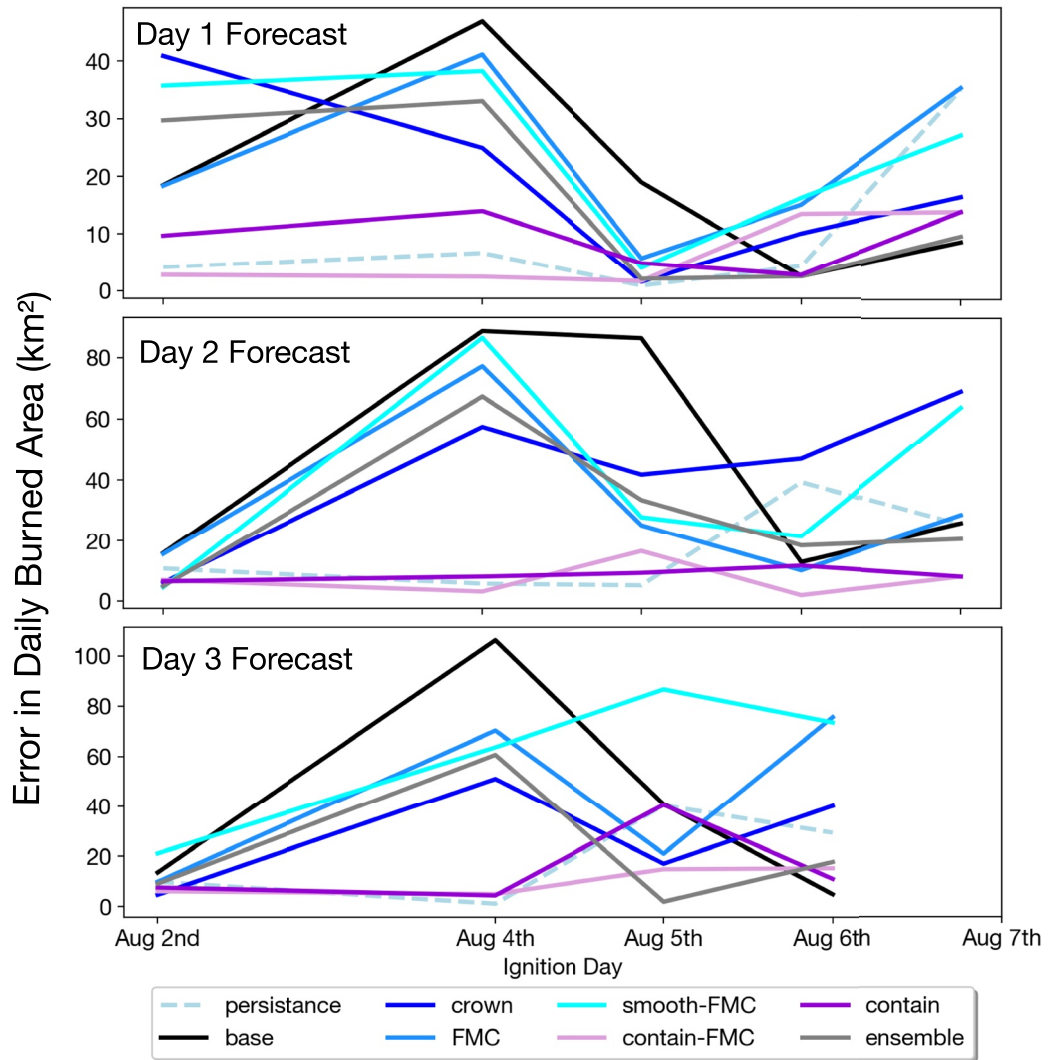


**Figure 7.** Absolute difference between WRF-Fire and NIROPS on daily burned area for different ignition days and different lengths of time into the simulation. There are no 3-day forecasts for August 7th as the fire had been mostly contained by August 9th.

*base* configuration (Figure 8b). Despite our fuel density scaling correction and even though fire counts may be high or daily burned area accurate, the FRP can still be underpredicted. This might be due to uncertainties in fuel type, fuel density, radiant heat fraction, or some combination of factors.

Another discrepancy we see with FRP comparisons is overprediction of nighttime burning for some simulations (Figure 8b; Figure 15 in Supporting Information S1), which may be due in part to the lack of a dynamic, or time variable, fuel moisture scheme in this study (Hiers et al., 2019; Moinuddin et al., 2021). Meteorological conditions at Williams Flats over the 7th and 8th enhanced the nocturnal fire activity (Peterson et al., 2022), which is reflected in the GOES-17 data and partially captured by WRF-Fire simulations (Figure 8), albeit overpredicted.

We found it was common in this study for modeled FRP to be out of phase with observation, usually with fire activity starting and ending too soon. To quantify this lead time, we looked at cross-correlations between WRF-Fire and GOES-17 FRP curves. To measure just the correlation in the broad day-night burning signal we removed much of the noise in FRP data. All simulated FRP curves were smoothed with a 12th degree Savitsky-Golay filter, Min-max normalized, and had early morning burning from the modeled FRP curves removed due to unrealistic nighttime burning from the previous day (Figure 9). We then estimated the lead time from modeled to

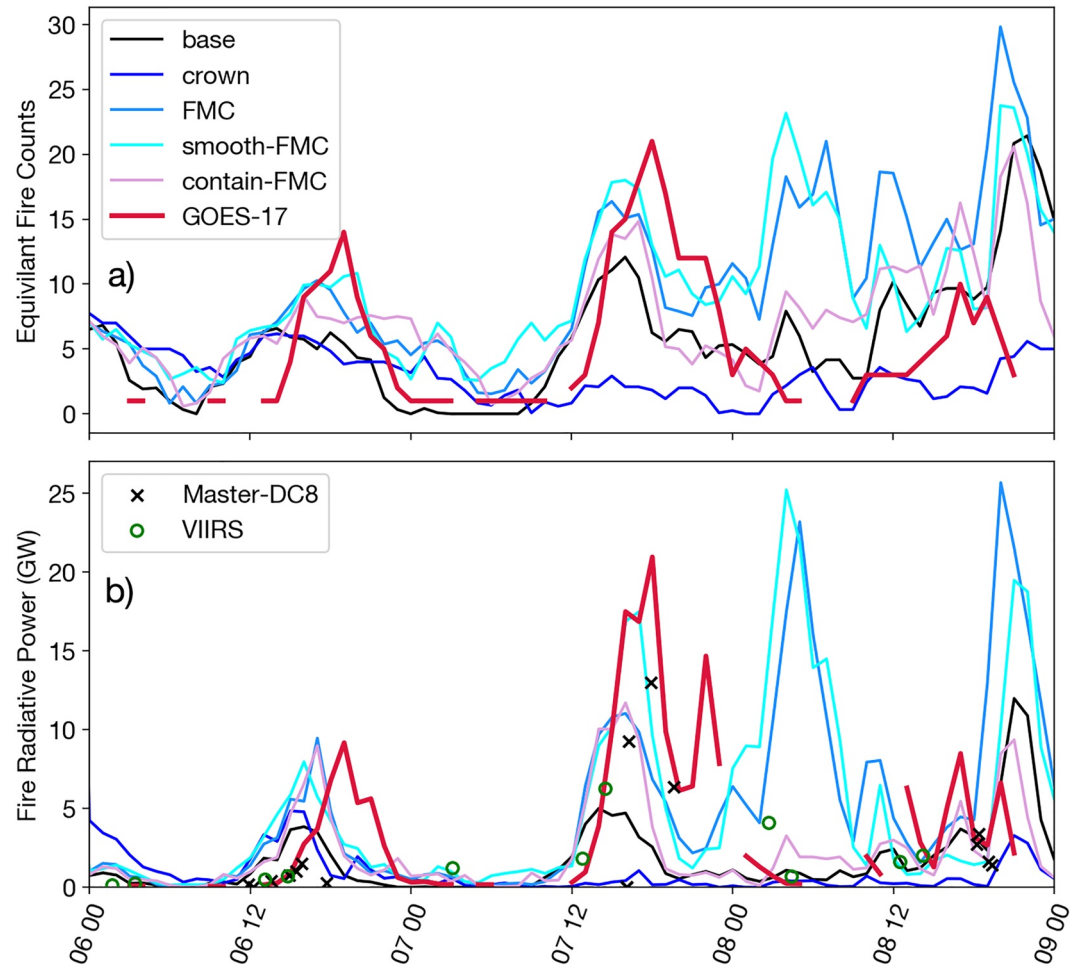


**Figure 8.** Simulations starting from a real perimeter ignition on 6 August 2019. (a), Fire counts, either from GOES-17 directly or with WRF-Fire heat data re-gridded and modeled after GOES-17 fire count retrieval (Section 2.5). (b): Fire Radiative Power (FRP) for all simulations, GOES-17 retrievals, VIIRS retrievals, or the master data from the DC-8 airplane flown in the joint NASA-NOAA 2019 campaign FIREX-AQ.

observed FRP curve by selecting the offset time which yielded the maximum correlation coefficient. Here we found that, on average, all models and prescribed temporal cycles led FRP retrievals by at least an hour, which increased with forecast day (Figure 10). On average, WRF-Fire's accuracy in temporal cycle is only comparable to the prescribed diurnal cycle that performed the best (HRRR-Smoke) when containment is applied, fuel moisture maps are used, and fuel density is scaled up simultaneously (i.e., *contain-fmc* simulation). Although WRF and nearby RAWS surface wind speeds led, or peaked earlier in the day than, GOES-17 FRP temporal cycles, surface Air Temperature ( $T$ ) and Relative Humidity (RH) lagged behind FRP, peaking or hitting a low later in the day (Figures S8 and S9 in Supporting Information S1).

#### 4. Discussion

It is not uncommon for studies to report model biases in overpredicting fire spread and although the mechanisms behind it may be difficult to identify, fuel models are often implicated as the cause (Dahl et al., 2015; Salis et al., 2016). Here we observe a general bias toward overestimation of burned area with some notable exceptions in simulations that were ignited or burned late into the fire, had increased fuel density, or accounted for containment. The inclusion of FMC maps created larger overpredictions at times as observed conditions were drier than what WRF prescribed by default. This is remedied however when used in conjunction with containment and fuel density scaling which then led to the most accurate results overall. Conversely, when modeling containment and

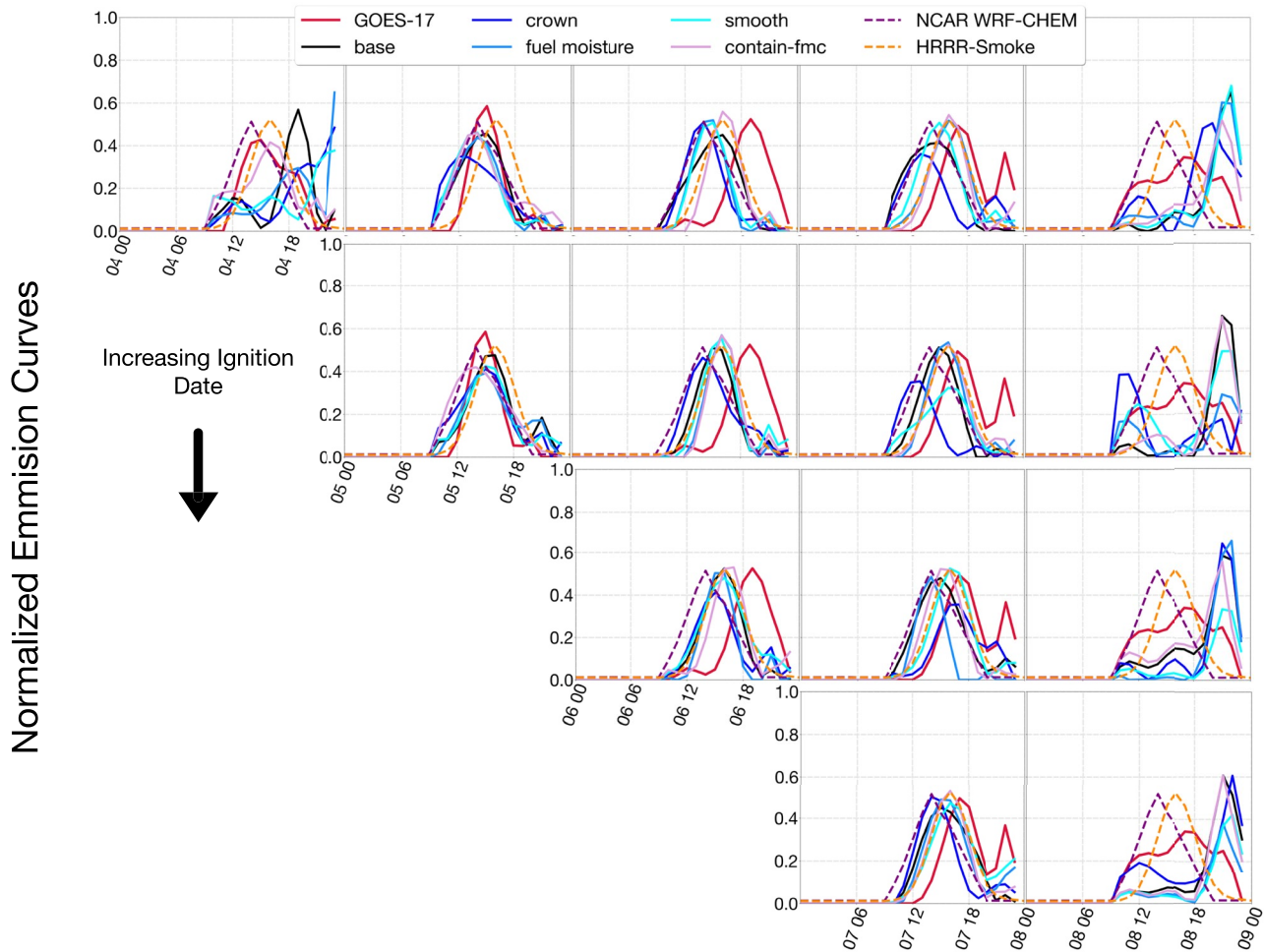


**Figure 9.** Normalized temporal cycles by time into simulation and day ignited. WRF-Fire simulations and GOES-17 data are interpolated, smoothed, and zeroed out in the early hours of the day to improve correlation statistics for Figure 10. NCAR WRF-CHEM and HRRR-Smoke are prescribed temporal cycles for smoke emission modeling, often used in conjunction with persistence forecasting (Section 2.5).

increasing fuel density without fuel moisture maps, we see an underestimation of burned area (*crown* and *contain*, Figures 3 and 5) implying fuel moisture maps generally create more accurate forecasts when containment and fuel density increases are incorporated as well. Thus, our results indicate that increasing realism in all aspects simultaneously (moisture, heat release and containment efforts) is needed to achieve optimal results.

Increasing fuel density to account for crown fires played a role in reducing fire spread where it was part of the configuration. Simulations with increased fuel density but without the fuel moisture maps had significantly less fire spread than the base in the forested regions (Figures 2 and 3) and at times ended in relative stagnation (Figure 3). This is to be expected as higher density fuels spread slower, release more heat and create a stronger convection sink in the center of the plume, potentially inhibiting fire spread (Quaife & Speer, 2021). These results show that WRF-Fire and other coupled models are sensitive to canopy fire modeling and fuel density characteristics. Thus, future work needs to implement canopy burning in a more explicit way (e.g., burning canopy and surface fuels independently) to assess effect into fire spread and heat release. Some of this work is already underway (Shamsaei et al., 2023).

In this study, modeling containment had the highest impact in reducing burned area overestimation with the caveat that we have a relatively idealistic way of accounting for containment, where all fire lines are assumed to be completed at the start of the simulation (Section 2.3). While this assumption was necessary for our study, future work could include more accurate containment dynamics. Despite this, these results, and the presence of significant containment efforts (Figure 1) suggest that for this fire, containment likely played a large role in

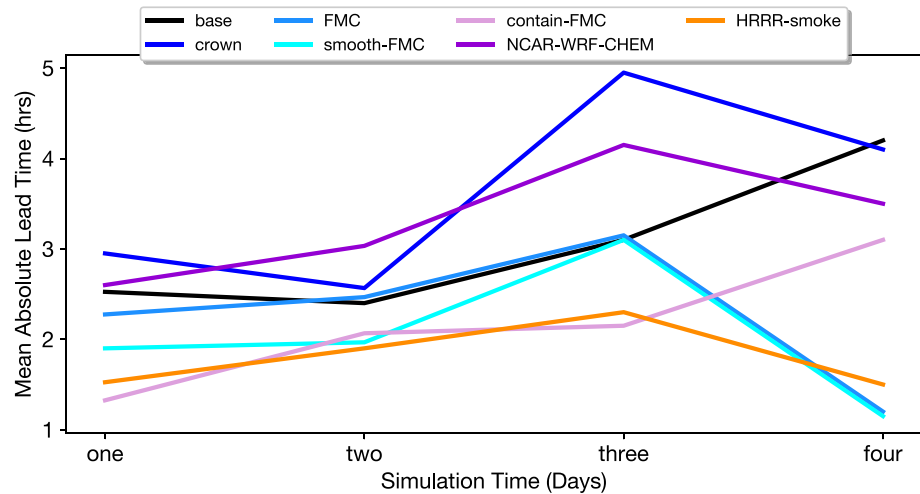


**Figure 10.** Time series of mean absolute lead time between WRF-Fire simulations, smoke emission model prescriptions, and GOES-17 temporal cycles (Figure 9). Lead time is the offset of cross correlation that produces the maximum correlation coefficient. Although we show the absolute offset here, it's almost always the case that the model temporal cycles led observations, perhaps in part do our static fuel moisture input (Section 4). See Table 1 and/or Section 2.4 for breakdown of the models.

reducing the spread of the fire, and without modeling containment, overestimation is likely to occur when forecasting burned area. Access to near-real time information on completed and planned fire lines would facilitate the inclusion of this information when these tools are used in forecasting mode.

Without modeled containment, simulations tend to overestimate fire-spread until the later days of the fire where intense burn days occurred. In these final days of the fire, steep topography, lack of roads, a large burnt-out interior, and proximity to the river bend may have made containment difficult or not needed, resulting in few containment lines in the forested mountain ridges (Figure 1) and improved accuracy for non-containment simulations (Figures 6 and 7). Once these factors are in place, we can see that not only are non-containment runs frequently more accurate than persistence, but also the *ensemble* mean can be more accurate than the containment runs (Figure 7).

The same configurations that increased accuracy in burned area and FRP (i.e., *contain-fmc*) also increased accuracy in predicting temporal cycles, despite still consistently leading the observations. In general, WRF-Fire and prescribed smoke emission curves both predict the fire as picking up too early in the day and dying off too early at night. Because the modeled temporal curves do not seem to get less out phase with observation as the fire is ignited later into the fire (Figure 9), more accurate meteorology or fire perimeters are perhaps unlikely to be the main driving factor in the lag we observe. One factor influencing this could be the lack of dynamic fuel moisture modeling in this study as fuel may not properly dampen when the temperature drops at night. Indeed, from comparisons between WRF and RAWS data (Figures S8–S10 in Supporting Information S1), it appears that although simulated and observed surface wind speeds lead observed FRP, often picking up in the morning, surface RH and T don't reach their minimum and maximum, respectively, until the afternoon. This supports the idea that the FRP temporal curve is shifted later into the day by the cycle of relative humidity and temperature that modulate fuel moisture content and which is missing in our simulations. New releases of WRF-Fire contain a dynamic fuel moisture model that could be assessed in future work.

A few real-world insights are implied from the difference between WRF-Fire configurations in this study. Based on the impact that containment modeling makes in this study, it's very likely the effort by fire-fighters along the southern and western flanks of the fire, specifically hand lines, dozer lines, and roads as lines, were effective in preventing a much larger wildfire. In this fire, containment lines in flat grasslands may have been easier for fire crews to implement compared to steep forests but the results here indicate that such efforts likely make a large difference in containing the overall fire spread anyway. We believe that the development of a near-real-time public data repository for current and planned containment lines and/or the addition of more accurate timestamps in the historical archives have the potential to greatly improve smoke and wildfire modeling efforts.



## 5. Conclusions

Wildfire forecasting remains a challenging task in both operational and research settings. Here we've partially alleviated this by assessing WRF-Fire's sensitivity to different model configurations. Inputs such as FMC, scaled fuel densities, and containment lines were incorporated into the model in different configurations and the results were compared against common forecasting metrics. Daily burned area and FRP were calculated and compared to standard methods of forecasting such as persistence and assumed temporal cycles. Results suggest that certain configuration options can be the difference between outperforming standard forecasting methods or incurring significant error, with containment modeling being the most important for this fire.

We found that WRF-Fire can be more accurate than persistence in burned area, and thus improve smoke forecasting skill, when used with sufficiently realistic input conditions. The combination of incorporating novel inputs in containment, fuel moisture, and fuel density in one configuration yielded the best results, with 30% less error than persistence on daily burned area over a 5-day forecast. To a lesser degree, using an ensemble forecast, igniting later into the fire, or forecasting for big fire growth days also helped in improving upon persistence. When used as inputs, satellite derived fuel moisture maps improve accuracy in daily burned area occasionally, but only when combined with containment and fuel density increases do they provide a consistent boost in accuracy.

This trend continued into our analysis of diurnal cycles, where accounting for containment, fuel moisture, and fuel density increases showed the most skill in capturing temporal cycles and heat output. Under these best-case configurations, WRF-Fire matches the accuracy of prescribed diurnal cycles used in air quality models. We found that increasing the fuel density, especially when FMC balanced out the reduced fire spread, improved WRF-Fire's FRP outputs significantly.

On average, all WRF-Fire temporal cycles and smoke emission model cycles commence too early in the day by at least an hour, and although the cause is not completely clear, a further investigation into dynamic fuel moisture schemes could help to illuminate this. In addition, we found simulations that accounted for FMC could produce nighttime burning similar to GOES-17 observations but often overestimated. With the increase of nocturnal burning under climate change (Balch et al., 2022) dynamic fuel moisture and nighttime burning could be important for future studies.

From a methodological standpoint, this study has established several important comparisons between simulation and observation. We have shown that WRF-Fire can be compared against GOES-17 fire count and FRP after re-gridding to the GOES-17 grid and accounting for the radiant heat fraction. Several insights have been drawn from this comparison including that the WRF-Fire default configuration does not release enough heat compared to satellite observation. In addition, our sensitivity study on WRF-Fire's second domain time step, or by proxy, the number of re-initializations per second of the level set function, was a previously unexplored topic in real fire simulation studies and shows the need for future studies to carefully consider time step choice on a case-by-case basis.

## Data Availability Statement

The official repository for WRF, which includes WRF-Fire configurations, is through GitHub (*WRF: The official repository for the Weather Research and Forecasting (WRF) model*, 2021). The WRF Pre-processing System (WPS) is also available through GitHub (*WPS: The official repository for the WRF Preprocessing System (WPS)*, 2021). The Open Wildland Fire Modeling E-community maintains a guide on WRF-Fire which was useful for this project ([https://wiki.openwfm.org/wiki/How\\_to\\_run\\_WRF-Fire\\_with\\_real\\_data](https://wiki.openwfm.org/wiki/How_to_run_WRF-Fire_with_real_data)).

Input data for WRF-Fire is open source and described in-text. The High-Resolution Rapid Refresh (HRRR) model (Dowell et al., 2022) output is archived in grib2 format at the University of Utah [https://home.chpc.utah.edu/~u0553130/Brian\\_Blaylock/hrrr\\_FAQ.html](https://home.chpc.utah.edu/~u0553130/Brian_Blaylock/hrrr_FAQ.html) (Blaylock & Horel, 2021; B. K. Blaylock et al., 2017). High-resolution topography and fuel categories can be found on the LANDFIRE data distribution site (Department of Interior, Geological Survey, and U.S. Department of Agriculture, 2016; Ryan & Opperman, 2013). The fuel moisture content maps are archived by the National Center for Atmospheric Research (NCAR) and Geoscience Data Exchange (GDEx) (Kosovic et al., 2019). Containment data and fire perimeters can be found at the National Interagency Fire Center (NIFC) Open Data Site (Wildland Fire Interagency Data Service (WFIGS), National Interagency Fire Center (NIFC), National Wildfire Coordinating Group (NWCG) Geospatial

Subcommittee, 2021). Perimeters as well as intense heat and scattered heat partitions can be found on the NIFC Public Access Folder in Incident Specific Data (<https://ftp.wildfire.gov/>). RAWs data can be accessed through an open access online portal (Western Regional Climate Center, 2023).

To insert a fire perimeter and remove the fuel in the non-intense heat regions on the wrfinput\_d02 file, we used the following open source python libraries:

- netCDF4.Dataset is used to read and overwrite variables in wrfinput\_d02. We read in the variable LFN\_HIST and overwrite it with the imprinted perimeter,
- json is used to read the polygon geometry coordinates in the perimeter file (in geojson format),
- matplotlib.path.Path and matplotlib.path.contains\_points are used to mask points in/out of the fire perimeter,
- scipy.ndimage.distance\_transform\_edt is used to assign a value of 1 to points where the perimeter mask is True, and calculate the exact Euclidean distance between True points (inside of perimeter) and their closest False point (perimeter boundary). The resulting distances are reversed (1-x), yielding a new LFN\_HIST field where negative values indicate points inside the perimeter,
- shapely.geometry.polygon.contains is used to check if grid cells are within the intense heat areas for fuel removal.

The calculation of GOES-17 grid cell centers followed this tutorial on MakerPortal (<https://makersportal.com/blog/2018/11/25/goes-r-satellite-latitude-and-longitude-grid-projection-algorithm>). GOES-17 Wildfire Automated Biomass Burning Algorithm (WFABBA) FRP product is generated by the Cooperative Institute for Meteorological Satellite Studies (CIMSS) at the University of Wisconsin, Madison. GOES-17 fire detections and FRP data for this study, as well as DC-8 measurements are archived by NASA/LARC/SD/ASDC (NASA/LARC/SD/ASDC, 2020).

The following open source python libraries were used for data analysis in this study:

- salem.open\_mf\_wrf\_dataset was used to open multiple WRF output files in a single xarray.dataset,
- pyproj.transform was used with cartopy contours of FIRE\_AREA (WRF-Fire output) to project shapely.geometry.polygon fire perimeters (Equal Area Cylindrical) for burned area calculations,
- geopandas was used to open and project NIROPS shape files (Equal Area Cylindrical) for burned area calculations,
- matplotlib.path.Path and matplotlib.path.contains\_points were used to check if WRF-Fire grid cells were within GOES-17's grid cells
- scipy.signal.correlate was used to create the cross correlation matrix from which offset in FRP temporal cycle was calculated,

Matplotlib v3.1.3 (Caswell et al., 2020) and Cartopy 0.17.0 (Elson et al., 2022) were used to create the 2-dimensional figures in this paper. The Visualization and Analysis Platform for Ocean, Atmosphere, and Solar Researchers (VAPOR) was used to make 3-dimensional contour plots of Q-Criterion (Li et al., 2019).

A sample case has been made available for this study with Zenodo (Turney, 2023). This contains much of the inputs and outputs from the *contain-FMC* simulation ignited just before August 6th. Found there is the information needed to run WRF-Fire including the configurations files *namelist.input* and *namelist.fire*.

#### Acknowledgments

This work was supported through an NSF Graduate Student Research Fellowship as well as Grants NSF 2013461, NOAA NA18OAR4310107, and NASA 80NSSC18K0629. Collaboration and funding from the National Center for Atmospheric Research and the Naval Research Laboratory also aided this project immensely. We also want to thank Melinda Berman for supplying us with data products for VIIRS fire area.

#### References

- Abatzoglou, J. T., & Williams, A. P. (2016). Impact of anthropogenic climate change on wildfire across western US forests. *Proceedings of the National Academy of Sciences of the United States of America*, 113(42), 11770–11775. <https://doi.org/10.1073/pnas.1607171113>
- Ahmadv, R., Grell, G., James, E., Csiszar, I., Tsidulko, M., Pierce, B., et al. (2017). Using VIIRS fire radiative power data to simulate biomass burning emissions, plume rise and smoke transport in a real-time air quality modeling system. In *2017 IEEE international geoscience and remote sensing symposium (IGARSS)* (pp. 2806–2808). Retrieved from [ieeexplore.ieee.org](http://ieeexplore.ieee.org)
- Anderson, D. H., Catchpole, E. A., De Mestre, N. J., & Parkes, T. (1982). Modelling the spread of grass fires. *ANZIAM Journal*, 23(4), 451–466. <https://doi.org/10.1017/s0334270000000394>
- Anderson, H. E. (1981). *Aids to determining fuel models for estimating fire behavior*. U.S. Department of Agriculture, Forest Service, Intermountain Forest and Range Experiment Station.
- Andrews, P. L. (2014). Current status and future needs of the BehavePlus fire modeling system. *International Journal of Wildland Fire*, 23(1), 21. <https://doi.org/10.1071/wf12167>
- Bakhshaii, A., & Johnson, E. A. (2019). A review of a new generation of wildfire-atmosphere modeling. *Canadian Journal of Forest Research*, 49(6), 565–574. <https://doi.org/10.1139/cjfr-2018-0138>
- Balch, J. K., Abatzoglou, J. T., Joseph, M. B., Koontz, M. J., Mahood, A. L., McGlinchy, J., et al. (2022). Warming weakens the night-time barrier to global fire. *Nature*, 602(7897), 442–448. <https://doi.org/10.1038/s41586-021-04325-1>
- Benjamin, S. G., Weygandt, S. S., Brown, J. M., Hu, M., Alexander, C. R., Smirnova, T. G., et al. (2016). A North American hourly assimilation and model forecast cycle: The rapid refresh. *Monthly Weather Review*, 144(4), 1669–1694. <https://doi.org/10.1175/mwr-d-15-0242.1>

- Berman, M., Ye, X., Thapa, L., Peterson, D., Hyer, E., Soja, A., et al. (2021). Quantifying burned area of wildfires from satellite active fire detections. In *AGU fall meeting* (Vol. 2021). Retrieved from <https://ui.adsabs.harvard.edu/abs/2021AGUFM.U55A..08B>
- Blaylock, B., & Horel, J. (2021). Metadata for the high resolution rapid refresh model archives [Dataset]. HIVE. <https://doi.org/10.7278/S5JQ0Z5B>
- Blaylock, B. K., Horel, J. D., & Liston, S. T. (2017). Cloud archiving and data mining of high-resolution rapid refresh forecast model output [Dataset]. *Computers & Geosciences*, *109*, 43–50. <https://doi.org/10.1016/j.cageo.2017.08.005>
- Byram (1959). Combustion of forest fuels. *Forest fire: Control and use*. Retrieved from <https://ci.nii.ac.jp/naid/10029316165/>
- Caswell, T. A., Droettboom, M., Lee, A., Hunter, J., Firing, E., Stansby, D., et al. (2020). matplotlib/matplotlib v3.1.3 [Software]. Zenodo. <https://doi.org/10.5281/zenodo.3633844>
- Chopp, D. L. (1991). In J. Sethian (Ed.), *Computing minimal surfaces via level set curvature flow*. University of California. Retrieved from <https://www.proquest.com/dissertations-theses/computing-minimal-surfaces-via-level-set/docview/303917093/se-2>
- Clark, T. L., Coen, J., & Latham, D. (2004). Description of a coupled atmosphere–fire model. *International Journal of Wildland Fire*, *13*(1), 49–63. <https://doi.org/10.1071/wf03043>
- Coen, J. L. (2005). Simulation of the Big Elk Fire using coupled atmosphere–fire modeling. *International Journal of Wildland Fire*, *14*(1), 49–59. <https://doi.org/10.1071/wf04047>
- Coen, J. L., Cameron, M., Michalakos, J., Patton, E. G., Riggan, P. J., & Yedinak, K. M. (2013). WRF-Fire: Coupled weather–wildland fire modeling with the weather research and forecasting model. *Journal of Applied Meteorology and Climatology*, *52*(1), 16–38. <https://doi.org/10.1175/jamc-d-12-023.1>
- Dahl, N., Xue, H., Hu, X., & Xue, M. (2015). Coupled fire–atmosphere modeling of wildland fire spread using DEVS-FIRE and ARPS. *Natural Hazards*, *77*(2), 1013–1035. <https://doi.org/10.1007/s11069-015-1640-y>
- Deardorff, J. W. (1980). Stratocumulus-capped mixed layers derived from a three-dimensional model. *Boundary-Layer Meteorology*, *18*(4), 495–527. <https://doi.org/10.1007/bf00119502>
- De Moura, C. A., & Kubrusly, C. S. (2013). The Curant–Friedrichs–Lewy (CFL) condition.
- Department of Interior, Geological Survey, and U.S. Department of Agriculture. (2016). LANDFIRE: LANDFIRE 13 fire behavior fuel models-Anderson [Dataset]. [Online]. LANDFIRE 40 Fire Behavior Fuel Models-Scott/Burgan, Elevation (2020, Last Update). Retrieved from <http://landfire.cr.usgs.gov/viewer/>
- Dobrinkova, N., & Dobrinkov, G. (2014). FARSITE and WRF-fire models, Pros and Cons for Bulgarian cases. In *Large-scale scientific computing* (pp. 382–389). Springer Berlin Heidelberg.
- Dowell, D. C., Alexander, C. R., James, E. P., Weygandt, S. S., Benjamin, S. G., Manikin, G. S., et al. (2022). The high-resolution rapid refresh (HRRR): An hourly updating convection-allowing forecast model. Part I: Motivation and system Description. *Weather and Forecasting*, *37*(8), 1371–1395. <https://doi.org/10.1175/waf-d-21-0151.1>
- Drury, S. A., Narasimhan Sim Larkin, T. T. S., Huang, S., Strenfel, S. J., Banwell, E. M., O'Brien, T. E., et al. (2014). Intercomparison of fire size, fuel loading, fuel consumption, and smoke emissions estimates on the 2006 Tripod fire. *Fire Ecology*, *10*, 56–83. <https://doi.org/10.4996/fireecology.1001056>
- Elson, P., de Andrade, E. S., Lucas, G., May, R., Hattersley, R., Campbell, E., et al. (2022). SciTools/cartopy: v0.21.1 [Software]. Zenodo. <https://doi.org/10.5281/zenodo.7430317>
- Finney, M. A. (1998). *FARSITE, fire area simulator—model development and evaluation*. U.S. Department of Agriculture, Forest Service, Rocky Mountain Research Station.
- Frankman, D., Webb, B. W., Butler, B. W., Jimenez, D., Forthofer, J. M., Sopko, P., et al. (2012). Measurements of convective and radiative heating in wildland fires. *International Journal of Wildland Fire*, *22*(2), 157–167. <https://doi.org/10.1071/wf11097>
- Frediano, M., Juliano, T. W., DeCastro, A., Kosovic, B., & Kniewel, J. (2021). A fire-spotting parameterization coupled with the WRF-fire model. *Earth and Space Science Open Archive*. <https://doi.org/10.1002/essoar.10506771.1>
- Freeborn, P. H., Wooster, M. J., Hao, W. M., Ryan, C. A., Nordgren, B. L., Baker, S. P., & Ichoku, C. (2008). Relationships between energy release, fuel mass loss, and trace gas and aerosol emissions during laboratory biomass fires. *Journal of Geophysical Research*, *113*(D1), D01301. <https://doi.org/10.1029/2007jd008679>
- Graff, C. A., Coffield, S. R., Chen, Y., Foufloula-Georgiou, E., Randerson, J. T., & Smyth, P. (2020). Forecasting daily wildfire activity using Poisson regression. *IEEE Transactions on Geoscience and Remote Sensing: A Publication of the IEEE Geoscience and Remote Sensing Society*, *58*(7), 4837–4851. <https://doi.org/10.1109/tgrs.2020.2968029>
- Halofsky, J. E., Peterson, D. L., & Harvey, B. J. (2020). Changing wildfire, changing forests: The effects of climate change on fire regimes and vegetation in the Pacific Northwest, USA. *Fire Ecology*, *16*(1), 4. <https://doi.org/10.1186/s42408-019-0062-8>
- Hiers, J. K., Stauhammer, C. L., O'Brien, J. J., Gholz, H. L., Martin, T. A., Hom, J., & Starr, G. (2019). Fine dead fuel moisture shows complex lagged responses to environmental conditions in a saw palmetto (*Serenoa repens*) flatwoods. *Agricultural and Forest Meteorology*, *266*–267, 20–28. <https://doi.org/10.1016/j.agrformet.2018.11.038>
- Jimenez, P. A., Brown, B., Kosovic, B., Cowie, J., Munoz-Esparza, D., Anderson, A., et al. (2018). Description and evaluation of the Colorado fire prediction system (CO-FPS) (p. EP31B–03). Retrieved from [ui.adsabs.harvard.edu](https://ui.adsabs.harvard.edu)
- Johnston, J. M., Wooster, M. J., Paugam, R., Wang, X., Lynham, T. J., & Johnston, L. M. (2017). Direct estimation of Byram's fire intensity from infrared remote sensing imagery. *International Journal of Wildland Fire*, *26*(8), 668–684. <https://doi.org/10.1071/wf16178>
- Juliano, T. W., Kosović, B., Jiménez, P. A., Eghdami, M., Haupt, S. E., & Martilli, A. (2022). “Gray Zone” simulations using a three-dimensional planetary boundary layer parameterization in the weather research and forecasting model. *Monthly Weather Review*, *150*(7), 1585–1619. <https://doi.org/10.1175/mwr-d-21-0164.1>
- Kochanski, A. K., Herron-Thorpe, F., Mallia, D. V., Mandel, J., & Vaughan, J. K. (2021). Integration of a coupled fire-atmosphere model into a regional air quality forecasting system for wildfire events. *Frontiers in Forests and Global Change*, *4*. <https://doi.org/10.3389/ffgc.2021.728726>
- Kochanski, A. K., Jenkins, M. A., Mandel, J., Beezley, J. D., Clements, C. B., & Krueger, S. (2013). Evaluation of WRF-SFIRE performance with field observations from the FireFlux experiment. *Geoscientific Model Development*, *6*(4), 1109–1126. <https://doi.org/10.5194/gmd-6-1109-2013>
- Kosovic, B. (2021). WPS-GEO-LocalFilter: Python scripts for local filtering of terrain heights in WPS geo\_em\* files created by geogrid.exe [Software]. Github. Retrieved from <https://github.com/brankokosovic/WPS-GEO-LocalFilter>
- Kosović, B., Jimenez, P., & McCandless, T. (2020). Estimation of fuel moisture content by integrating surface and satellite observations using machine learning. IGARSS 2020-2020. Retrieved from [https://ieeexplore.ieee.org/abstract/document/9323134/?casa\\_token=Ry-zhr34S48YAAAAA:ncKoFH9fH0Wp8diNdVyw\\_pdyCMmd409hallxweDSOHmY\\_JlahDu\\_mZlYzOIEB-8My45cfUxr7c](https://ieeexplore.ieee.org/abstract/document/9323134/?casa_token=Ry-zhr34S48YAAAAA:ncKoFH9fH0Wp8diNdVyw_pdyCMmd409hallxweDSOHmY_JlahDu_mZlYzOIEB-8My45cfUxr7c)
- Kosovic, B., Massie, S., McCandless, T., Petzke, B., Jimenez Munoz, P., DeCastro, A., & Siems-Anderson, A. (2019). Fuel moisture content (live and dead) over the conterminous United States. Version 1.0 [Dataset]. UCAR/NCAR - GDEX. <https://doi.org/10.5065/qt42-zd40>

- Kumar, R., Bhardwaj, P., Pfister, G., Drews, C., Honomichl, S., & D'Attilo, G. (2021). Description and evaluation of the fine particulate matter forecasts in the NCAR regional air quality forecasting system. *Atmosphere*, *12*(3), 302. <https://doi.org/10.3390/atmos12030302>
- Lee, G.-J., Muñoz-Esparza, D., Yi, C., & Choe, H. J. (2019). Application of the cell perturbation method to large-eddy simulations of a real urban area. *Journal of Applied Meteorology and Climatology*, *58*(5), 1125–1139. <https://doi.org/10.1175/jamc-d-18-0185.1>
- Li, F., Zhang, X., Kondragunta, S., Lu, X., Csiszar, I., & Schmidt, C. C. (2022). Hourly biomass burning emissions product from blended geostationary and polar-orbiting satellites for air quality forecasting applications. *Remote Sensing of Environment*, *281*, 113237. <https://doi.org/10.1016/j.rse.2022.113237>
- Li, F., Zhang, X., Kondragunta, S., Schmidt, C. C., & Holmes, C. D. (2020). A preliminary evaluation of GOES-16 active fire product using Landsat-8 and VIIRS Active fire data, and ground-based prescribed fire records. *Remote Sensing of Environment*, *237*, 111600. <https://doi.org/10.1016/j.rse.2019.111600>
- Li, S., Jaroszynski, S., Pearse, S., Orf, L., & Clyne, J. (2019). VAPOR: A visualization package tailored to analyze simulation data in earth system science [Software]. *Atmosphere*, *10*, 488. <https://doi.org/10.3390/atmos10090488>
- Mandel, J., Amram, S., Beezley, J. D., Kelman, G., Kochanski, A. K., Kondratenko, V. Y., et al. (2014). New features in WRF-SFIRE and the wildfire forecasting and danger system in Israel. *Natural Hazards and Earth System Sciences Discussions*, *2*(2), 1759–1797.
- Mandel, J., Beezley, J. D., & Kochanski, A. K. (2011). Coupled atmosphere-wildland fire modeling with WRF-Fire. arXiv [physics.ao-ph]. Retrieved from <http://arxiv.org/abs/1102.1343>
- Matt Jolly, W. (2007). Sensitivity of a surface fire spread model and associated fire behavior fuel models to changes in live fuel moisture. *International Journal of Wildland Fire*, *16*(4), 503–509. <https://doi.org/10.1071/wf06077>
- McCaffrey, S., McGee, T. K., Coughlan, M., & Tedim, F. (2020). 8 - Understanding wildfire mitigation and preparedness in the context of extreme wildfires and disasters: Social science contributions to understanding human response to wildfire. In F. Tedim, V. Leone, & T. K. McGee (Eds.), *Extreme wildfire events and disasters* (pp. 155–174). Elsevier.
- Moinuddin, K., Khan, N., & Sutherland, D. (2021). Numerical study on effect of relative humidity (and fuel moisture) on modes of grassfire propagation. *Fire Safety Journal*, *125*, 103422. <https://doi.org/10.1016/j.firesaf.2021.103422>
- Muñoz-Esparza, D., Kosović, B., Jiménez, P. A., & Coen, J. L. (2018). An accurate fire-spread algorithm in the weather research and forecasting model using the level-set method. *Journal of Advances in Modeling Earth Systems*, *10*(4), 908–926. <https://doi.org/10.1002/2017ms001108>
- NASA/LARC/SD/ASDC. (2020). FIREX-AQ DC-8 in-situ aerosol data [Dataset]. NASA Langley Atmospheric Science Data Center DAAC. [https://doi.org/10.5067/ASDC/FIREXAQ\\_Aerosol\\_AircraftInSitu\\_DC8\\_Data\\_1](https://doi.org/10.5067/ASDC/FIREXAQ_Aerosol_AircraftInSitu_DC8_Data_1)
- Peterson, D., Hyer, E., & Wang, J. (2013). A short-term predictor of satellite-observed fire activity in the North American boreal forest: Toward improving the prediction of smoke emissions. *Atmospheric Environment*, *71*, 304–310. <https://doi.org/10.1016/j.atmosenv.2013.01.052>
- Peterson, D., Wang, J., Ichoku, C., Hyer, E., & Ambrosia, V. (2013). A sub-pixel-based calculation of fire radiative power from MODIS observations: 1: Algorithm development and initial assessment. *Remote Sensing of Environment*, *129*, 262–279. <https://doi.org/10.1016/j.rse.2012.10.036>
- Peterson, D. A., Thapa, L. H., Saide, P. E., Soja, A. J., Gargulinski, E. M., Hyer, E. J., et al. (2022). Measurements from inside a thunderstorm driven by wildfire: The 2019 FIREX-AQ field experiment. *Bulletin of the American Meteorological Society*. <https://doi.org/10.1175/bams-d-21-0049.1>
- Preisler, H. K., & Westerling, A. L. (2007). Statistical model for forecasting monthly large wildfire events in western United States. *Journal of Applied Meteorology and Climatology*, *46*(7), 1020–1030. <https://doi.org/10.1175/jam2513.1>
- Quaife, B., & Speer, K. (2021). A simple model for wildland fire vortex-sink interactions. *Atmosphere*, *12*(8), 1014. <https://doi.org/10.3390/atmos12081014>
- Rai, R. K., Berg, L. K., Kosović, B., Haupt, S. E., Mirocha, J. D., Ennis, B. L., & Draxl, C. (2019). Evaluation of the impact of horizontal grid spacing in terra incognita on coupled mesoscale-microscale simulations using the WRF framework. *Monthly Weather Review*, *147*(3), 1007–1027. <https://doi.org/10.1175/mwr-d-18-0282.1>
- Rothermel, R. C. (1972). *A mathematical model for predicting fire spread in wildland fuels*. Intermountain Forest & Range Experiment Station, Forest Service, U.S. Department of Agriculture.
- Ryan, K. C., & Opperman, T. S. (2013). LANDFIRE—A national vegetation/fuels data base for use in fuels treatment, restoration, and suppression planning. *Forest Ecology and Management*, *294*, 208–216. <https://doi.org/10.1016/j.foreco.2012.11.003>
- Salis, M., Arca, B., Alcasena, F., Arianoutsou, M., Bacciu, V., Duce, P., et al. (2016). Predicting wildfire spread and behaviour in Mediterranean landscapes. *International Journal of Wildland Fire*, *25*(10), 1015–1032. <https://doi.org/10.1071/wf15081>
- Schmidt, C. (2020). Monitoring fires with the GOES-R series. In *The GOES-R series* (pp. 145–163). Elsevier.
- Schroeder, W., & Giglio, L. (2017). Visible infrared imaging radiometer suite (VIIRS) 375 m & 750 m active fire detection data sets based on NASA VIIRS land science investigator processing system (SIPS) reprocessed data -version 1 product user's guide version 1.3. Retrieved from [https://lpdaac.usgs.gov/documents/132/NP14\\_User\\_Guide\\_v1.3.pdf](https://lpdaac.usgs.gov/documents/132/NP14_User_Guide_v1.3.pdf)
- Scott, J. H. (2005). *Standard fire behavior fuel models: A comprehensive set for use with Rothermel's surface fire spread model*. U.S. Department of Agriculture, Forest Service, Rocky Mountain Research Station.
- Shamsaei, K., Juliano, T. W., Roberts, M., Ebrahimian, H., Lareau, N. P., Rowell, E., & Kosovic, B. (2023). The role of fuel characteristics and heat release formulations in coupled fire-atmosphere simulation. Preprints. <https://doi.org/10.20944/preprints202305.1672.v1>
- Skamarock, W. C., Klemp, J. B., Dudhia, J., Gill, D. O., Liu, Z., Berner, J., et al. (2019). A description of the advanced research WRF Version 4. NCAR Tech. Note NCAR/TN-556+STR (p. 145). <https://doi.org/10.5065/1dfh-6p97>
- Sussman, M., Smereka, P., & Osher, S. (1994). A level set approach for computing solutions to incompressible two-phase flow. *Journal of Computational Physics*, *114*(1), 146–159. <https://doi.org/10.1006/jcph.1994.1155>
- Thapa, L. H., Ye, X., Hair, J. W., Fenn, M. A., Shingler, T., Kondragunta, S., et al. (2022). Heat flux assumptions contribute to overestimation of wildfire smoke injection into the free troposphere. *Communications Earth & Environment*, *3*(1), 1–11. <https://doi.org/10.1038/s43247-022-00563-x>
- Turney, F. (2023). Williams flats WRF-fire output contain for FMC [Dataset]. Zenodo. <https://doi.org/10.5281/zenodo.7693759>
- Tymstra, C., Bryce, R. W., Wotton, B. M., Taylor, S. W., Armitage, O. B., & Others (2010). *Development and structure of Prometheus: The Canadian wildland fire growth simulation model information report NOR-X-417*. (Edmonton, AB). Natural Resources Canada, Canadian Forest Service, Northern Forestry Centre. Retrieved from [http://epe.lac-bac.gc.ca/100/200/301/nrcan-ncan/cfs-scf/nor-x/dev\\_structure\\_prometheus/31775.pdf](http://epe.lac-bac.gc.ca/100/200/301/nrcan-ncan/cfs-scf/nor-x/dev_structure_prometheus/31775.pdf)
- Tymstra, C., Jain, P., & Flannigan, M. D. (2021). Characterisation of initial fire weather conditions for large spring wildfires in Alberta, Canada. *International Journal of Wildland Fire*, *30*(11), 823–835. <https://doi.org/10.1071/wf21045>
- Wang, Q., Ihme, M., Linn, R. R., Chen, Y.-F., Yang, V., Sha, F., et al. (2022). A high-resolution large-eddy simulation framework for wildfire predictions using TensorFlow. arXiv [physics.flu-dyn]. Retrieved from <http://arxiv.org/abs/2212.05141>

- Western Regional Climate Center. (2023). RAWS USA climate archive state selection map [Dataset]. Western Regional Climate Center. Retrieved from <https://raws.dri.edu/>
- Wiedinmyer, C., Akagi, S. K., Yokelson, R. J., Emmons, L. K., Al-Saadi, J. A., Orlando, J. J., & Soja, A. J. (2011). The fire INventory from NCAR (FINN): A high resolution global model to estimate the emissions from open burning. *Geoscientific Model Development*, 4(3), 625–641. <https://doi.org/10.5194/gmd-4-625-2011>
- Wiggins, E. B., Soja, A. J., Gargulinski, E., Halliday, H. S., Pierce, R. B., Schmidt, C. C., et al. (2020). High temporal resolution satellite observations of fire radiative power reveal link between fire behavior and aerosol and gas emissions. *Geophysical Research Letters*, 47(23). <https://doi.org/10.1029/2020gl090707>
- Wildland Fire Interagency Data Service (WFIGS), National Interagency Fire Center (NIFC), National Wildfire Coordinating Group (NWCG) Geospatial Subcommittee. (2021). Operational data archive 2019 [Dataset]. Wildland Fire Interagency Data Service (WFIGS), National Interagency Fire Center (NIFC), National Wildfire Coordinating Group (NWCG) Geospatial Subcommittee. Retrieved from <https://data-nifc.opendata.arcgis.com/>
- WPS. (2021). The official repository for the WRF Preprocessing System (WPS) [Software]. Github. Retrieved from <https://github.com/wrf-model/WPS>
- WRF. (2021). The official repository for the Weather Research and Forecasting (WRF) model [Software]. Github. Retrieved from <https://github.com/wrf-model/WRF>
- Wyngaard, J. C. (2004). Toward numerical modeling in the “Terra Incognita. *Journal of the Atmospheric Sciences*, 61(14), 1816–1826. [https://doi.org/10.1175/1520-0469\(2004\)061<1816:tnmitt>2.0.co;2](https://doi.org/10.1175/1520-0469(2004)061<1816:tnmitt>2.0.co;2)
- Xu, W., Wooster, M. J., He, J., & Zhang, T. (2021). Improvements in high-temporal resolution active fire detection and FRP retrieval over the Americas using GOES-16 ABI with the Geostationary Fire Thermal Anomaly (FTA) Algorithm. *Egyptian Journal of Remote Sensing and Space Sciences*, 3(June), 100016. <https://doi.org/10.1016/j.srs.2021.100016>
- Ye, X., Arab, P., Ahmadov, R., James, E., Saide, P. E., Pierce, B., et al. (2021). Evaluation and intercomparison of wildfire smoke forecasts from multiple modeling systems for the 2019 Williams Flats fire. *Atmospheric Chemistry and Physics*, 21(18), 14427–14469. <https://doi.org/10.5194/acp-21-14427-2021>
- Ye, X., Saide, P. E., daSilva, A., Kondragunta, S., Lyapustin, A., Wang, Y., et al. (2019). Evaluation of biomass burning smoke simulations incorporating near real-time inversions of multi-fire emissions over the Western U.S (p. A22A–07).
- Zigner, K., Carvalho, L. M. V., Peterson, S., Fujioka, F., Duine, G.-J., Jones, C., et al. (2020). Evaluating the ability of FARSITE to simulate wildfires influenced by extreme, downslope winds in Santa Barbara, California. *Fire*, 3(3), 29. <https://doi.org/10.3390/fire3030029>